RATE-ADAPTIVE QUANTIZATION: A MULTI-RATE CODEBOOK ADAPTATION FOR VECTOR QUANTIZED MODELS

Anonymous authors
Paper under double-blind review

ABSTRACT

Learning discrete representations with vector quantization (VQ) has emerged as a powerful approach in representation learning across vision, audio, and language. However, most VQ models rely on a single, fixed-rate codebook, requiring extensive retraining for new bitrates or efficiency requirements. We introduce *Rate-Adaptive Quantization (RAQ)*, a multi-rate codebook adaptation framework for VQ models. RAQ integrates a lightweight sequence-to-sequence (Seq2Seq) codebook generator with the base VQ model, enabling on-demand codebook adaptation to any target size at inference. Additionally, we provide a clustering-based post-hoc alternative for pre-trained VQ models, suitable when modifying the training pipeline or joint training is not feasible. Our experiments demonstrate that RAQ performs effectively across multiple rates and VQ models, often outperforming fixed-rate baselines. This model-agnostic adaptability enables a single system to meet varying bitrate requirements in reconstruction and generation tasks.

1 INTRODUCTION

Vector quantization (VQ) (Gray, 1984) is a fundamental technique for learning discrete representations for various tasks (Krishnamurthy et al., 1990; Gong et al., 2014; Van Niekerk et al., 2020) in the field of machine learning. The Vector Quantized Variational Autoencoder (VQ-VAE) (Van Den Oord et al., 2017; Razavi et al., 2019), which extends the encoder-decoder structure of the Variational Autoencoder (VAE) (Kingma & Welling, 2013; Rezende & Viola, 2018), introduces discrete latent representations that have proven effective across vision (Razavi et al., 2019; Esser et al., 2021), audio (Dhariwal et al., 2020; Yang et al., 2023), and speech tasks (Kumar et al., 2019; Xing et al., 2023). The inherently discrete nature of these modalities makes VQ particularly well-suited for complex inference and generation.

Recent developments have further enhanced VQ-based discrete representation learning by integrating it with deep generative models, such as Generative Adversarial Networks (GANs) (Esser et al., 2021) and Denoising Diffusion Probabilistic Models (DDPMs) (Cohen et al., 2022; Gu et al., 2022; Yang et al., 2023). As VQ models are integrated into these diverse generative frameworks, their utility and applicability in various tasks are becoming increasingly evident. However, even with these advancements, *scalability* remains a bottleneck. In practical settings such as live streaming, telepresence, and on-device applications, the available bandwidth and compute resources can fluctuate dramatically. A single fixed-rate VQ model either wastes bits when higher quality is possible or severely degrades fidelity under tight constraints. Maintaining separate VQ models for each bitrate is infeasible and incurs significant overhead. Hence, a robust framework that can seamlessly adapt its compression rate is crucial for real-world deployments.

Several works have explored enhancing the flexibility of codebooks. Li et al. (2023) introduced a codebook-resizing technique for publicly available VQ models by applying hyperbolic embeddings, Malka et al. (2023) propose a nested codebook to support multiple quantization levels, and multi-codebook vector quantization is used in speech (Guo et al., 2022) and a knowledge distillation setting (Guo et al., 2023). Recently, Huijben et al. (2024) focused on unsupervised codebook generation based on residual quantization by studying the vector quantizer itself. However, it remains impractical to increase the rate of an already-deployed quantizer by appending new residual

stages after training. Simply adding more codebooks tends to disrupt the learned latent distribution and often necessitates a reduction in the spatial/temporal resolution of feature maps. This post-hoc capacity-scaling bottleneck is what motivated the development of our RAQ framework, which adapts bit rates through a lightweight Seq2Seq module that generates new codebook embeddings, while leaving the original VQ architecture untouched.

In this paper, we present *Rate-Adaptive Quantization (RAQ)*, a framework designed to flexibly modulate the effective codebook size of a single VQ model without retraining. By incorporating a Sequence-to-Sequence (Seq2Seq) (Sutskever et al., 2014) into the VQ model, RAQ enables one system to cover multiple compression levels, reducing the need for separate models dedicated to each rate. This adaptability not only minimizes storage and maintenance costs but also provides a smoother user experience in real-time communications or streaming environments, where bandwidth availability can vary from moment to moment. While our main focus is on the Seq2Seq-based RAQ, we additionally propose a model-based alternative that applies differentiable k-means (DKM) (Cho et al., 2021) clustering to a pre-trained VQ model, offering codebook adaptation when joint training or architectural modification is not feasible. This simple approach provides a practical fallback in scenarios where retraining or model modification is not feasible.

Our contributions are summarized as follows:

- We propose the *Rate-Adaptive Quantization (RAQ)* framework for flexible multi-rate codebook adaptation, using a Sequence-to-Sequence (Seq2Seq) module to generate codebook embeddings of any target size without retraining. This method can be integrated into existing VQ models with minimal modifications.
- To mitigate distribution mismatch in autoregressive Seq2Seq codebook adaptation, we introduce a *cross-forcing* training procedure. This approach ensures stable codebook generation across diverse rates and enhances reconstruction fidelity.
- We evaluate RAQ on several VQ benchmarks and show that a *single* RAQ-enabled model consistently meets or exceeds the performance of multiple fixed-rate VQ baselines while using the same encoder-decoder architecture.

2 Background

2.1 Vector-Quantized Variational AutoEncoder

VQ-VAEs (Van Den Oord et al., 2017) can successfully represent meaningful features that span multiple dimensions of data space by discretizing continuous latent variables to the nearest codebook vector in the codebook. In a VQ model, learning of discrete representations is achieved by quantizing the encoded latent variables to their nearest neighbors in a trainable codebook and decoding the input data from the discrete latent variables. To represent the data $\mathbf{x}$ from dataset $\mathcal{D}$ discretely, a codebook $\mathbf{e}$ consisting of K learnable codebook vectors $\{e_i\}_{i=1}^{K} \subset \mathbb{R}^d$ is employed (where d denotes the dimensionality of each codebook vector e_i). The quantized discrete latent variable $\mathbf{z}_q(\mathbf{x}|\mathbf{e})$ is decoded to reconstruct the data $\mathbf{x}$. The vector quantizer Q is modeled as a deterministic categorical posterior that maps each spatial position $[m, n]$ of the continuous latent representation $\mathbf{z}_e(\mathbf{x})[m, n]$ of the data $\mathbf{x}$ by a deterministic encoder f_ϕ to $\mathbf{z}_q(\mathbf{x}|\mathbf{e})[m, n]$ by finding the nearest neighbor from the codebook $\mathbf{e} = \{e_i\}_{i=1}^{K}$ as

$$\mathbf{z}_q(\mathbf{x}|\mathbf{e})[m, n] = Q\Big(\mathbf{z}_e(\mathbf{x})[m, n]\Big|\mathbf{e}\Big) = \arg\min_i \|\mathbf{z}_e(\mathbf{x})[m, n] - e_i\|\,, \tag{1}$$

The quantized representation uses $\log_2 K$ bits to index one of the K selected codebook vectors $\{e_i\}_{i=1}^{K}$. The deterministic decoder f_θ reconstructs the data $\mathbf{x}$ from the quantized discrete latent variable $\mathbf{z}_q(\mathbf{x}|\mathbf{e})$ as $\hat{\mathbf{x}} = f_\theta\big(\mathbf{z}_q(\mathbf{x}|\mathbf{e})|\mathbf{e}\big)$. During the training process, the encoder f_ϕ, decoder f_θ, and codebook $\mathbf{e}$ are jointly optimized to minimize the loss $\mathcal{L}_{\text{VQ}}\big(\phi, \theta, \mathbf{e}; \mathbf{x}\big) =$

$$\underbrace{\log p_\theta(\mathbf{x}|\mathbf{z}_q(\mathbf{x}|\mathbf{e}))}_{\mathcal{L}_{\text{recon}}} + \underbrace{\big|\big|\text{sg}\big[f_\phi(\mathbf{x})\big] - \mathbf{z}_q(\mathbf{x}|\mathbf{e})\big|\big|_2^2}_{\mathcal{L}_{\text{embed}}} + \underbrace{\beta\big|\big|\text{sg}\big[\mathbf{z}_q(\mathbf{x}|\mathbf{e})\big] - f_\phi(\mathbf{x})\big|\big|_2^2}_{\mathcal{L}_{\text{commit}}} \tag{2}$$

where $\text{sg}[\cdot]$ is the *stop-gradient* operator. The $\mathcal{L}_{\text{recon}}$ is the reconstruction loss between the input data $\mathbf{x}$ and the reconstructed decoder output $\hat{\mathbf{x}}$. The two $\mathcal{L}_{\text{embed}}$ and $\mathcal{L}_{\text{commit}}$ losses apply only to codebook variables and encoder weights with a weighting hyperparameter β to prevent fluctuations from

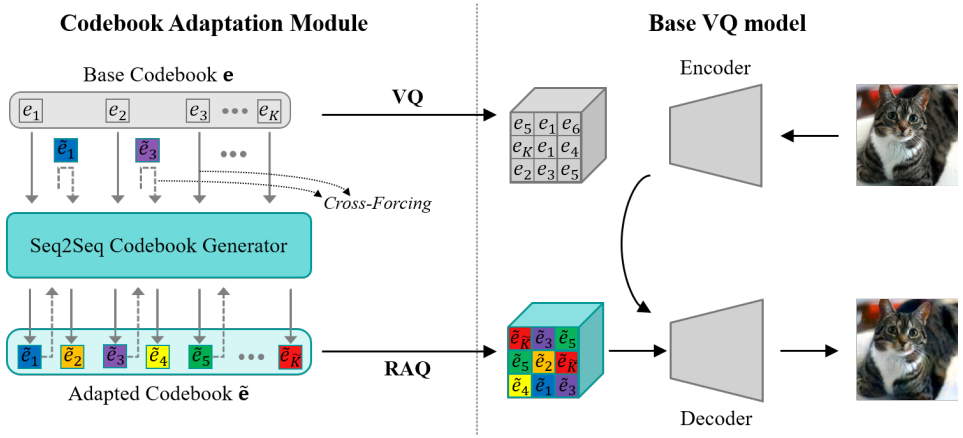

Figure 1: An overview of our RAQ framework applied to a base VQ model. During training, the codebook adaptation module employs cross-forcing to generate adapted codebooks $\tilde{\mathbf{e}}$ for randomly sampled sizes $\widetilde{K}$ from the base codebook $\mathbf{e}$. At inference, a user-specified target $\widetilde{K}$ produces the corresponding adapted codebook for rate-adaptive quantization.

one codebook vector to another. Since the quantization process is non-differentiable, the codebook loss is typically approximated via a straight-through gradient estimator (Bengio et al., 2013), such as $\partial\mathcal{L}/\partial f_\phi(\mathbf{x}) \approx \partial\mathcal{L}/\partial \mathbf{z}_q(\mathbf{x})$. Both conventional VAE (Kingma & Welling, 2013) and VQ-VAE (Van Den Oord et al., 2017) have objective functions consisting of the sum of reconstruction error and latent regularization. To improve performance and convergence rate, an exponential moving average (EMA) update is usually applied for the codebook optimization (Van Den Oord et al., 2017; Razavi et al., 2019). Thus, VQ models serve as a foundation for many advanced generative models, forming the core approach to discrete latent representation.

2.2 Sequence-to-Sequence Learning

The Seq2Seq (Sutskever et al., 2014) model is widely used in sequence prediction tasks such as language modeling and machine translation (Dai & Le, 2015; Luong et al., 2016; Ranzato et al., 2016). The model employs an initial LSTM, called the encoder, to process the input sequence $x_{1:N}$ sequentially and produce a substantial fixed-dimensional vector representation, called the context vector. The output sequence $y_{1:T}$ is then derived by a further LSTM, the decoder. A Seq2Seq with parameters ψ estimates the distribution of output sequence $y_{1:T}$ by decomposing it into an ordered product of conditional probabilities:

$$p(y_{1:T}|x_{1:N};\psi) = \prod_{t=1}^{T} p(y_t|y_{1:t-1}, x_{1:N};\psi) \tag{3}$$

During training, the Seq2Seq model typically uses *teacher-forcing* (Williams & Zipser, 1989), where the target sequence is provided to the decoder at each time step, instead of the decoder using its own previous output as input. This method helps the model converge faster by providing the correct context during training.

3 Methods

Although VQ models have demonstrated strong performance across modalities, their fixed codebook size can limit adaptability under varying data characteristics or resource constraints. In practice, the choice of the codebook size K (a key hyperparameter in VQ models) can vary widely with (i) on the application domain (e.g., small codebooks, $K \approx 8$, in certain audio domains (Chae et al., 2025)), (ii) input dimensionality and resolution (e.g., image generation models report K from 512 up to 16,384 (Esser et al., 2021)), and (iii) the model architecture and quantization scheme. This variability often forces practitioners to retrain or maintain multiple VQ models at different rates. To address these challenges, we introduce the RAQ framework, which adjusts a VQ model's rate

by increasing or decreasing the codebook size K on demand. We formalize RAQ as a mapping $\Psi : \mathbb{R}^{d\times K} \longrightarrow \mathbb{R}^{d\times \widetilde{K}}$ for any integer $\widetilde{K} \in \mathbb{N}$. We next detail a Seq2Seq-based RAQ strategy, followed by a model-based (clustering) alternative.

3.1 Rate-Adaptive Quantization

Overview The RAQ framework is designed to integrate seamlessly with existing VQ models without requiring significant architectural modifications. As illustrated in Figure 1, RAQ is integrated into a base VQ model which consists of an encoder-decoder pair and a trainable base codebook $\mathbf{e}$. The adapted codebook $\tilde{\mathbf{e}}$ is generated by a Seq2Seq model from the base codebook $\mathbf{e}$. During training, $\widetilde{K}$ is randomly sampled under a cross-forcing strategy. At inference, a user-specified target $\widetilde{K}$ is used to generate the codebook on demand.

Scope and Compatibility with Vector Quantizers RAQ exclusively operates at the quantization layer of existing VQ models and applies to any quantizer that uses a vector-embedding-based discrete representation. Hierarchical VQ (Razavi et al., 2019), stochastic quantization (Takida et al., 2022), residual quantization (Huijben et al., 2024), and linear-transformed VQ (Zhu et al., 2024) are some of the representative examples. Importantly, RAQ does not alter the base training procedure or the overall architecture. Unlike autoregressive token predictors (Esser et al., 2021; Yu et al., 2022; Huijben et al., 2024), which generate discrete index sequences under fixed codebook embeddings, RAQ synthesizes the codebook itself.

Autoregressive Generation of Adapted Codebooks Our codebook adaptation module G_ψ maps a base codebook $\mathbf{e}$ to an adapted codebook $\tilde{\mathbf{e}}$ via an Seq2Seq model. Each base codebook vector e_i of $\mathbf{e}$ is treated analogously to a token in language modeling. We train the Seq2Seq module to produce a set of $\widetilde{K}$ adapted codebook embeddings. This autoregressive generation ensures that each $\tilde{e}_i$ is conditioned on the previously generated vectors, promoting coherence and structural consistency. Formally, the adapted codebook is generated as

$$p\big(\tilde{\mathbf{e}}|\mathbf{e};\psi\big) = \prod_{i=1}^{\widetilde{K}} p\big(\tilde{e}_i|\tilde{e}_{<i}, e_{1:K};\psi\big) \tag{4}$$

where $\tilde{e}_{<i}$ denotes the vectors generated before step i. Unlike typical Seq2Seq setups that optimize next-token likelihood, the order of $\tilde{e}_{i:\widetilde{K}}$ is not semantically meaningful here; what matters is the distribution of embeddings. Accordingly, RAQ trains the Seq2Seq module with the base VQ objective computed using $\tilde{\mathbf{e}}$ (e.g., reconstruction or perceptual losses), tying codebook generation directly to downstream reconstruction quality without imposing an arbitrary sequence order or introducing extra losses.

Codebook Encoding We begin by initializing the target codebook size $\widetilde{K}$. During training, $\widetilde{K}$ is randomly sampled from a predefined range at each iteration. Each base codebook vector e_i is sequentially processed by LSTM cells, whose hidden and cell states $(\boldsymbol{h}, \boldsymbol{c})$ summarize context over the base codebook. This encoding captures dependencies among the base embeddings and provides a foundation for generating a coherent adapted codebook.

Codebook Decoding via Cross-Forcing We decode with a *cross-forcing* strategy that alternates teacher forcing and free running strategy to stably generate variable-size codebooks. Standard teacher forcing (Williams & Zipser, 1989) can be brittle when the target adapted codebook $\tilde{\mathbf{e}}$ is much longer than the base codebook, amplifying exposure bias. Cross-forcing mitigates this by interleaving the two modes, akin to professor forcing (Lamb et al., 2016). During training, the cross-forcing strategy operates as:

- **Teacher-Forcing Phase:** For odd indices i up to $2K$ (i.e., $1 \le i \le 2K$ and i is odd), the model uses the corresponding base codebook vector e_j as input, where $j = \frac{i+1}{2}$:

  $$\tilde{e}_i = \text{LSTM}_\psi(\tilde{e}_{<i}, e_j, \boldsymbol{h}, \boldsymbol{c}).$$

  This ensures that the fundamental distributional features of the base codebook are preserved during the early generation steps.

- **Free-Running Phase:** For even indices i up to $2K$ (i is even and $i \leq 2K$), and for all indices beyond $2K$ (i.e., $i > 2K$), the model relies on its previously generated adapted codebook vector $\tilde{e}_{i-1}$:
$$\tilde{e}_i = \text{LSTM}_\psi(\tilde{e}_{<i}, \tilde{e}_{i-1}, \boldsymbol{h}, \boldsymbol{c}).$$
By switching to its own outputs, the model learns to maintain coherence and consistency across the adapted codebook vectors for different sizes of $\widetilde{K}$.

Learning the codebook adaptation module G_ψ via cross-forcing is a key component of our RAQ. We provide an empirical evaluation of its effectiveness in Appendix A.3.2.

Training Procedure RAQ follows the objective of the base VQ model. Concretely, for a conventional VQ-VAE, let $\mathcal{L}_{\text{VQ}}$ (in equation 2) denote the standard loss. At each iteration, we sample a target size $\widetilde{K}$ from a predefined range, generate an adapted codebook $\tilde{\mathbf{e}} = G_\psi(\mathbf{e}; \widetilde{K})$, and jointly optimize $(\phi, \theta, \mathbf{e}, \psi)$ by minimizing a combined objective $(\mathcal{L}_{\text{VQ}} + \mathcal{L}_{\text{RAQ}})$, where $\mathcal{L}_{\text{RAQ}}\big(\phi, \theta, \psi, \mathbf{e}; \mathbf{x}\big) =$

$$\log p_\theta\big(\mathbf{x}|\mathbf{z}_q(\mathbf{x}|G_\psi(\mathbf{e}))\big) + \big|\big|\text{sg}\left[f_\phi(\mathbf{x})\right] - \mathbf{z}_q\big(\mathbf{x}|G_\psi(\mathbf{e})\big)\big|\big|_2^2 + \beta\big|\big|\text{sg}\left[\mathbf{z}_q\big(\mathbf{x}|G_\psi(\mathbf{e})\big)\right] - f_\phi\big(\mathbf{x}\big)\big|\big|_2^2. \quad (5)$$

Equivalently, RAQ trains by plugging the adapted codebook $\tilde{\mathbf{e}}$ into the existing objective function (no additional auxiliary losses are introduced). Sampling $\widetilde{K}$ each iteration exposes the model to multiple rates within a single training run.

3.2 Model-Based Rate-Adaptive Quantization (Alternative)

We present a post-hoc, model-based RAQ variant that adapts the codebook rate while leaving the rest of the base VQ model unchanged. Unlike the Seq2Seq-based RAQ, this approach adds no learnable modules; it directly resizes a pre-trained codebook $\mathbf{e}$ to a target $\widetilde{K}$ via clustering. Optional brief fine-tuning with the adapted codebook can be applied but is not required.

To obtain an adapted codebook $\tilde{\mathbf{e}}$ of size $\widetilde{K}$, we employ differentiable k-means (DKM) (Cho et al., 2021), originally proposed for compressing model weights via layer-wise clustering. Here, DKM is repurposed to cluster the embedding vectors in $\mathbf{e}$, yielding a reduced (or increased) codebook while preserving structure in the embedding space. We also leverage inverse functionalization (IKM) to accommodate increases in codebook size, enabling both rate reduction and rate expansion.

Codebook Reduction $(\widetilde{K} < K)$ In the rate-reduction task, DKM performs iterative, differentiable codebook clustering on $\widetilde{K}$ clusters. Let $\mathbf{C} = \{c_j\}_{j=1}^{\widetilde{K}}$ be the cluster centers for the base codebook $\mathbf{e}$ (Further details are provided in Appendix A.2.1). The process is as follows:

- Initialize the centroids $\mathbf{C} = \{c_j\}_{j=1}^{\widetilde{K}}$ by randomly selecting $\widetilde{K}$ codebook vectors from $\mathbf{e}$ or by using k-means++. The last updated $\mathbf{C}$ is used in subsequent iterations.
- Compute the Euclidean distance between each e_i and c_j, denoting $D_{i,j} = -f(e_i, c_j)$ to form the matrix $\boldsymbol{D}$.
- Form the attention matrix $\boldsymbol{A}$ via a softmax with temperature τ, where each row satisfies $A_{i,j} = \frac{\exp\left(\frac{D_{i,j}}{\tau}\right)}{\sum_k \exp\left(\frac{D_{i,k}}{\tau}\right)}$.
- Compute the candidate centroids $\widetilde{\mathbf{C}} = \{\tilde{c}_j\}$ by $\tilde{c}_j = \frac{\sum_i A_{i,j} e_i}{\sum_i A_{i,j}}$, then update $\mathbf{C} \leftarrow \widetilde{\mathbf{C}}$.
- Repeat until $\|\mathbf{C} - \widetilde{\mathbf{C}}\| \leq \epsilon$ or the iteration limit is reached. We then multiply $\boldsymbol{A}$ by $\mathbf{C}$ to obtain the final $\tilde{\mathbf{e}}$.

The above iterative process can be summarized as follows:

$$\tilde{\mathbf{e}} = \arg\min_{\tilde{\mathbf{e}}} \mathcal{L}_{\text{DKM}}(\mathbf{e}; \tilde{\mathbf{e}}) = \arg\min_{\mathbf{C}} |\mathbf{C} - \boldsymbol{A}\mathbf{C}| = \arg\min_{\mathbf{C}} \sum_{j=1}^{\widetilde{K}} \left| c_j - \frac{\sum_i A_{i,j} e_i}{\sum_i A_{i,j}} \right|. \quad (6)$$

Since the procedure is differentiable, the centroids and soft assignments can be optimized with a few steps of SGD. The temperature τ controls assignment hardness. After convergence, we assign each codebook vector to its nearest centroid according to the last attention matrix $\boldsymbol{A}$, thereby finalizing the compressed codebook.

Codebook Expansion ($\widetilde{K} > K$) As bandwidth and quality budgets increase, models benefit from a larger codebook, so codebook expansion must be supported. We propose an inverse functional DKM (IKM) method that grows the number of centroids from K to $\widetilde{K}$ and then refines them using the same DKM updates used in reduction. Algorithmic details and optimization choices are deferred to Appendix A.2.2.

Model-based RAQ operates directly on the codebook of any pre-trained VQ model, enabling post-hoc codebook rate adjustment without introducing new learnable modules. This approach is useful when training or integrating Seq2Seq-based RAQ is impractical. As it relies on differentiable clustering, fine-tuning is also supported via post-training. Appendix A.2.4 provides comparisons with alternative clustering methods and the effect of post-training.

4 Related Work

VQ and its Improvements The VQ-VAE (Van Den Oord et al., 2017) has inspired numerous developments since its inception. Łańcucki et al. (2020) and Zheng & Vedaldi (2023) proposed codebook reset and online clustering methods to mitigate *codebook collapse*, improving training efficiency. SQ-VAE (Takida et al., 2022) incorporated stochastic quantization and a trainable posterior categorical distribution to enhance VQ performance. Recently, SimVQ (Zhu et al., 2024) tackles the long-standing representation-collapse issue in vanilla VQ models by reparameterizing the codebook via linear transformation. Several works have introduced substantial structural changes to VQ modeling; for instance, RQ-VAE (Lee et al., 2022) employed a two-step residual quantization framework for high-resolution images, while FSQ (Mentzer et al., 2023) replaced VQ with finite scalar quantization to address codebook collapse. Our approach focuses on making rate-adaptive VQ without substantially altering the quantization mechanism or architecture, allowing it to scale effectively in both basic and advanced VQ models.

Variable-Rate Neural Image Compression Several studies have proposed variable-rate image compression based on autoencoders and VAEs (Yang et al., 2020; Choi et al., 2019; Cui et al., 2020), or using recurrent neural networks (Johnston et al., 2018). Song et al. (2021) introduced spatial feature transforms for compression, while Duong et al. (2023) combined learned transforms and entropy coding in a single model aligned with the rate-distortion curve. Variable-rate methods for discrete representation also exist. Dieleman et al. (2021) learn event-based codes with scalar quantization and control rate via channel budgets and target event rates, rather than resizing a fixed VQ codebook. In contrast, RAQ targets the VQ codebook itself. We adapt the vector embedding set to a user-specified size at inference without redesigning the underlying quantization mechanism or training a separate model per rate. Our RAQ directly addresses the practical need for a single VQ model to cover multiple bitrates.

5 Experiments

5.1 Experimental Setup

Settings We perform empirical evaluations on 3 vision datasets: CIFAR10 (Krizhevsky et al.) and CelebA (Liu et al., 2015), and ImageNet (Russakovsky et al., 2015). We use the same architecture and hyperparameters within each baseline model. The adapted codebook sizes range from 16 to 1024 for CIFAR10, 32 to 2048 for CelebA, and 32 to 4096 for ImageNet, while the base codebooks of baseline VQ models are fixed. RAQ-based models set the base codebook size to the middle of the range. We also provide details on each model's parameter count and complexity in Appendix A.2.5.

Evaluation Metrics We quantitatively evaluated our method using Peak-Signal-to-Noise-Ratio (PSNR), Structural Similarity Index Measure (SSIM), reconstructed Fréchet Inception Distance (rFID) (Heusel et al., 2017), Learned Perceptual Image Patch Similarity (LPIPS) (Zhang et al., 2018), and codebook perplexity. PSNR measures the ratio between the maximum possible power of a signal and the power of the corrupted noise affecting data fidelity (Korhonen & You, 2012). SSIM assesses structural similarity between two images (Wang et al., 2004). rFID and LPIPS assess the quality of reconstructed images by comparing the distribution of features extracted from

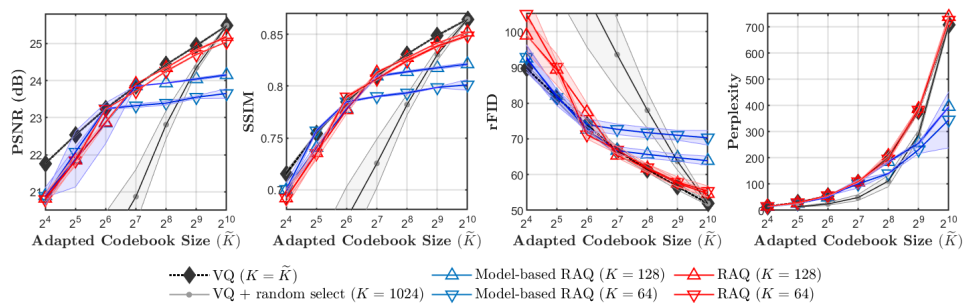

(a) CIFAR10 (32×32), baseline VQ model: VQ-VAE (Van Den Oord et al., 2017)

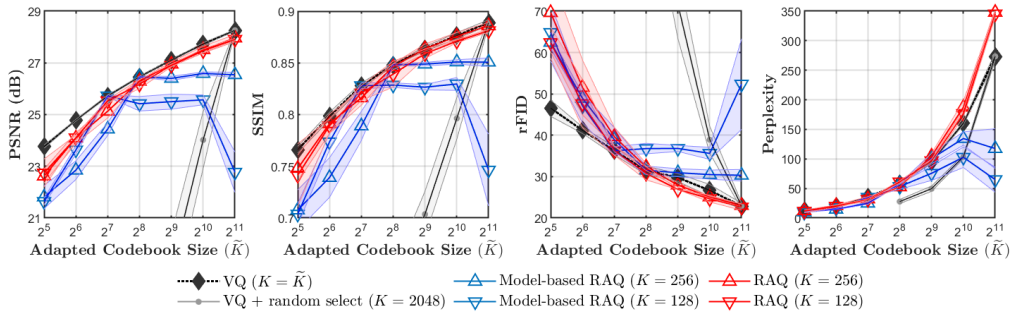

(b) CelebA (64×64), baseline model: VQ-VAE (Van Den Oord et al., 2017)

Figure 2: **Reconstruction results** on (a) CIFAR10 and (b) CelebA at various codebook sizes $\widetilde{K}$. The shaded area indicates the 95.45% confidence interval based on 4 runs with different seeds.

the test data with that of the original data. Codebook perplexity, defined as $e^{-\sum_i^{\widetilde{K}} p_{e_i} \log p_{e_i}}$ where $p_{e_i} = \frac{N_{e_i}}{\sum_j^{\widetilde{K}} N_{e_j}}$ and N_{e_i} represents the encoded number for latent representation with codebook e_i, indicates a uniform prior distribution when the perplexity value reaches the codebook size $\widetilde{K}$.

5.2 Quantitative Evaluation

We first empirically evaluate the effectiveness of RAQ using the vanilla VQ-VAE (Van Den Oord et al., 2017) on CIFAR10 and CelebA dataset. To establish a robust baseline, we trained multiple VQ-VAE models with varying codebook sizes K as fixed-rate benchmarks. We then tested RAQ's adaptability by dynamically adjusting the codebook size $\widetilde{K}$ within a single VQ-VAE. Figure 2 shows the comparative results.

RAQ closely matches the performance of multiple fixed-rate VQ-VAE models across most metrics, demonstrating its ability to maintain high reconstruction quality while offering rate flexibility. Specifically, under identical compression rates and network architectures, all RAQ variants achieve PSNR and SSIM scores nearly on par with their fixed-rate counterparts (e.g., within about 0.94 dB difference in PSNR on CIFAR10). When we increase the rate, RAQ occasionally shows slightly lower PSNR and SSIM but improves rFID, reflecting improved perceptual quality and better alignment with the dataset distribution. For instance, at $\widetilde{K} = 512$ on CelebA, rFID improves by up to about 9.6% compared to a fixed-rate VQ-VAE with the same codebook size, highlighting RAQ's ability to maintain visual coherence and realism in generative tasks. However, the model-based RAQ variant typically underperforms our Seq2Seq-based approach except in certain rate-reduction tasks. For further discussion of model-based RAQ, see Section 5.4.

We also evaluate RAQ across four representative VQ baselines (hierarchical VQ-VAE-2 (Razavi et al., 2019), stage-1 VQGAN (Esser et al., 2021), SQ-VAE (Takida et al., 2022), and SimVQ (Zhu et al., 2024)) to assess both rate flexibility and architectural generality. Table 1 reports mean PSNR, SSIM, LPIPS, and codebook perplexity over four runs. RAQ maintains or improves reconstruction quality relative to fixed-rate baselines while enabling on-demand adaptation of the codebook size.

On VQ-VAE-2, RAQ increases perplexity at higher rates while yielding comparable or better PSNR/LPIPS at mid–high $\widetilde{K}$. On stage-1 VQGAN, RAQ improves LPIPS in the mid-rate regime

Table 1: Performance comparison for *VQ-VAE-2* (Razavi et al., 2019), *stage-1 VQGAN* (Esser et al., 2021), *SQ-VAE* (Takida et al., 2022), and *SimVQ* (Zhu et al., 2024) with and without RAQ at multiple adapted codebook sizes $\widetilde{K}$. **Bold** indicates that the proposed method outperforms the baseline model, and the † denotes that the improvement is statistically indistinguishable from the baseline based on overlapping 95.45% confidence intervals.

Method	**VQ-VAE-2** / CelebA (128×128)						Method	**VQGAN** / ImageNet (256×256)					
	K	$\widetilde{K}$	PSNR↑	SSIM↑	LPIPS↓	Prplx.↑		K	$\widetilde{K}$	PSNR↑	SSIM↑	LPIPS↓	Prplx.↑
VQ-VAE-2	2048	–	33.37	0.9884	0.1050	334.7	VQGAN	512	–	21.00	0.7543	0.1000	296.3
VQ-VAE-2	1024	–	32.73	0.9865	0.1172	183.2	VQGAN	256	–	20.65	0.7383	0.1083	140.0
VQ-VAE-2	512	–	32.18	0.9842	0.1313	103.1	VQGAN	128	–	20.29	0.7221	0.1176	75.0
VQ-VAE-2	256	–	31.29	0.9810	0.1464	61.6	VQGAN	64	–	19.92	0.7015	0.1303	40.1
VQ-VAE-2	128	–	30.72	0.9780	0.1588	36.3	VQGAN	32	–	19.58	0.6834	0.1415	21.9
VQ-VAE-2 + random select	2048	1024	29.23	0.9717	0.1694	178.1	VQGAN + random select	512	256	19.98	0.7311	0.1185	148.5
		512	28.01	0.9642	0.2067	103.0			128	18.93	0.7035	0.1444	74.1
		256	26.43	0.9514	0.2584	60.4			64	17.37	0.6614	0.1917	37.2
		128	16.21	0.7266	0.5536	14.1			32	14.64	0.5801	0.3148	18.9
VQ-VAE-2 + **model -based RAQ**	2048	1024	31.62	0.9813	0.1404	131.1	VQGAN + **model -based RAQ**	512	256	20.43	0.7381	0.1119	147.1
		512	30.23	0.9733	0.1739	53.8			128	19.74	0.7182	0.1314	75.3
		256	29.09	0.9658	0.2068	30.6			64	18.82	0.6908	0.1642	39.6
		128	27.54	0.9518	0.2673	15.6			32	17.71	0.6546	0.2081	21.0
VQ-VAE-2 + **RAQ**	256	2048	33.26†	0.9881†	0.1097	**465.2**	VQGAN + **RAQ**	64	512	20.84	0.7415	0.1024	**311.4**
		1024	**32.77**	0.9865†	**0.1171**	**239.7**			256	20.61†	0.7332	**0.1079**	**159.7**
		512	**32.24**	**0.9847**	**0.1256**	**133.6**			128	20.26†	0.7207†	**0.1159**	**85.8**
		256	**31.33**	0.9809†	**0.1439**	**67.0**			64	19.86†	**0.7052**	**0.1283**	**45.0**
		128	30.39†	0.9771†	0.1663	**38.7**			32	19.03	0.6787	0.1554	**23.1**
	SQ-VAE / CelebA (128×128)							**SimVQ** / ImageNet (128×128)					
SQ-VAE	2048	–	32.04	0.9167	0.0911	449.40	SimVQ	4096	–	29.98	0.9109	0.1471	1667.61
SQ-VAE	1024	–	31.62	0.9141	0.0986	275.69	SimVQ	2048	–	29.71	0.9067	0.1536	987.94
SQ-VAE	512	–	30.96	0.9023	0.1088	149.17	SimVQ	1024	–	29.30	0.8986	0.1673	565.20
SQ-VAE	256	–	30.40	0.8927	0.1198	86.61	SimVQ	512	–	28.82	0.8882	0.1835	319.99
SQ-VAE	128	–	29.72	0.8786	0.1295	53.87	SimVQ	256	–	28.25	0.8747	0.2035	174.69
SQ-VAE	64	–	28.72	0.8613	0.1512	28.11	SimVQ	128	–	27.68	0.8601	0.2221	91.08
SQ-VAE + **RAQ**	128	2048	31.85	0.9142	0.0927	**521.19**	SimVQ + **RAQ**	512	4096	**30.03**	**0.9117**	0.1488	**2242.70**
		1024	31.40	0.9074	**0.0973**	269.29			2048	**29.74**	0.9066	0.1555	**1184.28**
		512	30.82	0.8990	**0.1041**	**156.03**			1024	**29.32**	**0.8990**	**0.1657**	**634.20**
		256	30.09	0.8905	**0.1156**	**90.36**			512	28.81	**0.8885**	**0.1810**	**334.01**
		128	28.95	0.8734	0.1352	**53.93**			256	28.19	0.8741	**0.2021**	**174.76**
		64	26.97	0.8356	0.1738	23.66			128	27.15	0.8503	0.2366	**92.15**

while staying within confidence bounds at extremes. For SQ-VAE and SimVQ (bottom blocks), RAQ consistently tracks or exceeds fixed-rate baselines across multiple $\widetilde{K}$. In contrast, random selection and the model-based variant degrade notably once more than half of the codebook is removed. These results indicate that RAQ's benefits extend beyond a single backbone and quantization scheme. Beyond reconstruction metrics, we observe systematically higher perplexity at larger $\widetilde{K}$ with RAQ, indicating more balanced code usage and richer latent capacity. Consistent with (Wu & Flierl, 2020; Takida et al., 2022; Vuong et al., 2023), increased codebook perplexity often correlates with better reconstruction. This improvement is especially evident at larger codebook sizes, where RAQ produces non-degenerate codebooks with broadly balanced usage, not just larger codebooks. This aligns with maximizing entropy in discrete representations and indicates that RAQ activates latent capacity underutilized by vanilla VQs.

In summary, RAQ offers substantial advantages in portability and reduced complexity. By consolidating multiple fixed-rate VQ models into a single adaptable framework, it saves training/storage overhead and simplifies deployment. Although minor trade-offs may appear at certain rates, the combination of flexibility and efficiency makes RAQ attractive across diverse VQ frameworks.

5.3 Qualitative Evaluation

For our qualitative evaluation, we visualize a single RAQ model based on VQ-VAE-2 (Razavi et al., 2019) reconstructing three Kodak (Kodak, 1993) images at four adapted codebook sizes (Figure 3). As the rate decreases, RAQ exhibits a smooth, graceful degradation: global shapes and hues remain stable while fine textures progressively become smoother. In the parrot (top row), the wrinkles marked with blue boxes remain sharp down to $\widetilde{K} = 256$. In the sailboat (middle row), the green-boxed sail numbers are clearly visible down to $\widetilde{K} = 256$. On the building facade (bottom row),

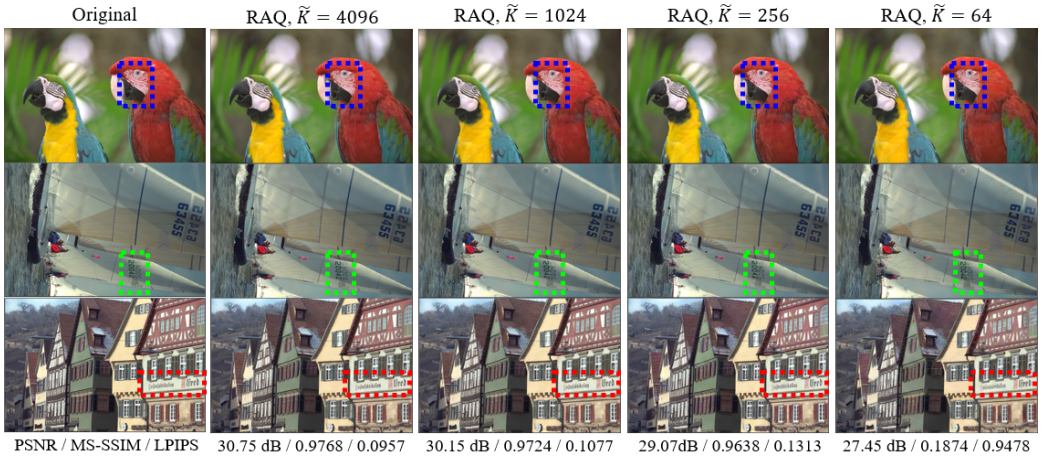

Figure 3: Multi-rate reconstructions with a single RAQ model. Three Kodak (768×512) images reconstructed at four codebook sizes. Colored boxes highlight fine details.

the text marked in red boxes maintains readability across all rates. Even at the lowest rate ($\widetilde{K} = 64$), all three images retain coherent structure and plausible colors. This demonstrates the superior effectiveness of our RAQ in handling variable-rate compression tasks, particularly in high-resolution image reconstruction scenarios. Further demonstrations can be found in Appendix A.3.7.

5.4 Discussion

Model-Based RAQ We also study a post-hoc, model-based variant that adapts rates without re-optimization, though its behavior depends on clustering dynamics. It is generally competitive for codebook reduction ($\widetilde{K} < K$) but shows sensitivity when expanding the codebook ($\widetilde{K} > K$) due to initialization, which can yield unstable assignments and suboptimal local minima (see Appendix A.2.3). In our supplementary study (Appendix A.2.4), plain DKM/k-means++/GMM achieve similar performance, whereas *DKM+post-training* closes much of the gap, suggesting a practical fallback when Seq2Seq-based RAQ is infeasible. Despite these limitations, model-based RAQ remains attractive in resource-constrained settings, since it only clusters the existing codebook and scales to large backbones (Yu et al., 2022) where retraining costs dominate.

Stage-2 Compatibility with Autoregressive Priors Unlike autoregressive token priors that predict index sequences under a fixed codebook, RAQ creates the codebook itself for any target $\widetilde{K}$ after training, leaving token modeling untouched. For completeness, we pair a single stage-1 RAQ-based VQ model with PixelCNN (van den Oord et al., 2016) and Transformer priors across multiple $\widetilde{K}$ (See Appendix A.3.1). These studies show competitive performance versus fixed-rate baselines while avoiding separate stage-1 retraining per rate, indicating that RAQ maintains stage-2 compatibility and downstream expressivity over multiple $\widetilde{K}$.

Additional Ablation Appendix A.3.2 ablates *cross-forcing*. When expanding the codebook ($\widetilde{K} > K$), it stabilizes generation and improves rFID (up to 4.9%) with modest PSNR/SSIM gains (Table 12). For $\widetilde{K} \leq K$, it can slightly underperform, reflecting its expansion-oriented design.

Computational Cost Please see Appendix A.2.6 for complexity experiments. RAQ unavoidably increases training time, but because a single model serves multiple rates, the overall cost remains practical. The latency to generate an adapted codebook for a target rate is only 10–140 ms, after which throughput is comparable to fixed-rate VQ models.

Conclusion In summary, RAQ enables multi-rate codebook adaptation across VQ models with a single stage-1 backbone while retaining compatibility with stage-2 priors. Remaining limitations include initialization sensitivity in model-based expansion and the need for deeper analysis, which we leave to future work.

Ethics Statement RAQ is designed as a rate-adaptive extension of VQ models and can be applied in all domains where VQ models are used. As with all generative models, attention should be given to potential biases in the training data, as these can affect generated outputs. RAQ does not introduce any new ethical concerns beyond those inherent in VQ models.

Reproducibility Statement Appendix A.1 provides details of the experiments. The complete code necessary to reproduce our experiments is included in the supplementary material.

REFERENCES

Yoshua Bengio, Nicholas Léonard, and Aaron Courville. Estimating or propagating gradients through stochastic neurons for conditional computation. *arXiv preprint arXiv:1308.3432*, 2013.

Yunkee Chae, Woosung Choi, Yuhta Takida, Junghyun Koo, Yukara Ikemiya, Zhi Zhong, Kin Wai Cheuk, Marco A. Martínez-Ramírez, Kyogu Lee, Wei-Hsiang Liao, and Yuki Mitsufuji. Variable bitrate residual vector quantization for audio coding. In *ICASSP 2025 - 2025 IEEE International Conference on Acoustics, Speech and Signal Processing (ICASSP)*, pp. 1–5, 2025.

Minsik Cho, Keivan Alizadeh-Vahid, Saurabh Adya, and Mohammad Rastegari. Dkm: Differentiable k-means clustering layer for neural network compression. In *International Conference on Learning Representations*, 2021.

Yoojin Choi, Mostafa El-Khamy, and Jungwon Lee. Variable rate deep image compression with a conditional autoencoder. In *Proceedings of the IEEE/CVF International Conference on Computer Vision*, pp. 3146–3154, 2019.

Max Cohen, Guillaume Quispe, Sylvain Le Corff, Charles Ollion, and Eric Moulines. Diffusion bridges vector quantized variational autoencoders. In *International Conference on Machine Learning*, pp. 4141–4156. PMLR, 2022.

Ze Cui, Jing Wang, Bo Bai, Tiansheng Guo, and Yihui Feng. G-vae: A continuously variable rate deep image compression framework. *arXiv preprint arXiv:2003.02012*, 2(3), 2020.

Andrew M Dai and Quoc V Le. Semi-supervised sequence learning. *Advances in neural information processing systems*, 28, 2015.

Prafulla Dhariwal, Heewoo Jun, Christine Payne, Jong Wook Kim, Alec Radford, and Ilya Sutskever. Jukebox: A generative model for music. *arXiv preprint arXiv:2005.00341*, 2020.

Sander Dieleman, Charlie Nash, Jesse Engel, and Karen Simonyan. Variable-rate discrete representation learning. *arXiv preprint arXiv:2103.06089*, 2021.

Lyndon R Duong, Bohan Li, Cheng Chen, and Jingning Han. Multi-rate adaptive transform coding for video compression. In *2023 IEEE International Conference on Acoustics, Speech and Signal Processing (ICASSP)*, pp. 1–5. IEEE, 2023.

Patrick Esser, Robin Rombach, and Bjorn Ommer. Taming transformers for high-resolution image synthesis. In *Proceedings of the IEEE/CVF conference on computer vision and pattern recognition*, pp. 12873–12883, 2021.

William A Falcon. Pytorch lightning. *GitHub*, 3, 2019.

Yunchao Gong, Liu Liu, Ming Yang, and Lubomir Bourdev. Compressing deep convolutional networks using vector quantization. *arXiv preprint arXiv:1412.6115*, 2014.

Robert Gray. Vector quantization. *IEEE Assp Magazine*, 1(2):4–29, 1984.

Arthur Gretton, Karsten M Borgwardt, Malte J Rasch, Bernhard Schölkopf, and Alexander Smola. A kernel two-sample test. *The Journal of Machine Learning Research*, 13(1):723–773, 2012.

Shuyang Gu, Dong Chen, Jianmin Bao, Fang Wen, Bo Zhang, Dongdong Chen, Lu Yuan, and Baining Guo. Vector quantized diffusion model for text-to-image synthesis. In *Proceedings of the IEEE/CVF Conference on Computer Vision and Pattern Recognition*, pp. 10696–10706, 2022.

Haohan Guo, Fenglong Xie, Frank K Soong, Xixin Wu, and Helen Meng. A multi-stage multi-codebook vq-vae approach to high-performance neural tts. In *Proceedings of INTERSPEECH*, 2022.

Liyong Guo, Xiaoyu Yang, Quandong Wang, Yuxiang Kong, Zengwei Yao, Fan Cui, Fangjun Kuang, Wei Kang, Long Lin, Mingshuang Luo, et al. Predicting multi-codebook vector quantization indexes for knowledge distillation. In *2023 IEEE International Conference on Acoustics, Speech and Signal Processing (ICASSP)*, pp. 1–5. IEEE, 2023.

Martin Heusel, Hubert Ramsauer, Thomas Unterthiner, Bernhard Nessler, and Sepp Hochreiter. Gans trained by a two time-scale update rule converge to a local nash equilibrium. *Advances in neural information processing systems*, 30, 2017.

Iris Huijben, Matthijs Douze, Matthew Muckley, Ruud van Sloun, and Jakob Verbeek. Residual quantization with implicit neural codebooks. *arXiv preprint arXiv:2401.14732*, 2024.

Nick Johnston, Damien Vincent, David Minnen, Michele Covell, Saurabh Singh, Troy Chinen, Sung Jin Hwang, Joel Shor, and George Toderici. Improved lossy image compression with priming and spatially adaptive bit rates for recurrent networks. In *Proceedings of the IEEE conference on computer vision and pattern recognition*, pp. 4385–4393, 2018.

Diederik P Kingma and Max Welling. Auto-encoding variational bayes. *arXiv preprint arXiv:1312.6114*, 2013.

Kodak. Kodak photocd dataset. 1993. URL `https://0k.us/graphics/kodak/`.

Jari Korhonen and Junyong You. Peak signal-to-noise ratio revisited: Is simple beautiful? In *2012 Fourth International Workshop on Quality of Multimedia Experience*, pp. 37–38, 2012.

Ashok K. Krishnamurthy, Stanley C. Ahalt, Douglas E. Melton, and Prakoon Chen. Neural networks for vector quantization of speech and images. *IEEE journal on selected areas in Communications*, 8(8):1449–1457, 1990.

Alex Krizhevsky, Vinod Nair, and Geoffrey Hinton. Cifar-10 (canadian institute for advanced research). URL `http://www.cs.toronto.edu/~kriz/cifar.html`.

Kundan Kumar, Rithesh Kumar, Thibault De Boissiere, Lucas Gestin, Wei Zhen Teoh, Jose Sotelo, Alexandre De Brebisson, Yoshua Bengio, and Aaron C Courville. Melgan: Generative adversarial networks for conditional waveform synthesis. *Advances in neural information processing systems*, 32, 2019.

Alex M Lamb, Anirudh Goyal ALIAS PARTH GOYAL, Ying Zhang, Saizheng Zhang, Aaron C Courville, and Yoshua Bengio. Professor forcing: A new algorithm for training recurrent networks. *Advances in neural information processing systems*, 29, 2016.

Adrian Łańcucki, Jan Chorowski, Guillaume Sanchez, Ricard Marxer, Nanxin Chen, Hans JGA Dolfing, Sameer Khurana, Tanel Alumäe, and Antoine Laurent. Robust training of vector quantized bottleneck models. In *2020 International Joint Conference on Neural Networks (IJCNN)*, pp. 1–7. IEEE, 2020.

Doyup Lee, Chiheon Kim, Saehoon Kim, Minsu Cho, and Wook-Shin Han. Autoregressive image generation using residual quantization. In *Proceedings of the IEEE/CVF Conference on Computer Vision and Pattern Recognition*, pp. 11523–11532, 2022.

Lei Li, Tingting Liu, Chengyu Wang, Minghui Qiu, Cen Chen, Ming Gao, and Aoying Zhou. Resizing codebook of vector quantization without retraining. *Multimedia Systems*, 29(3):1499–1512, 2023.

Ziwei Liu, Ping Luo, Xiaogang Wang, and Xiaoou Tang. Deep learning face attributes in the wild. In *Proceedings of International Conference on Computer Vision (ICCV)*, December 2015.

Ilya Loshchilov and Frank Hutter. Decoupled weight decay regularization. In *7th International Conference on Learning Representations, ICLR 2019, New Orleans, LA, USA, May 6-9, 2019*. OpenReview.net, 2019.

Minh-Thang Luong, Quoc V. Le, Ilya Sutskever, Oriol Vinyals, and Lukasz Kaiser. Multi-task sequence to sequence learning. In *4th International Conference on Learning Representations, ICLR 2016, May 2-4, Conference Track Proceedings*, 2016.

May Malka, Shai Ginzach, and Nir Shlezinger. Learning multi-rate vector quantization for remote deep inference. In *2023 IEEE International Conference on Acoustics, Speech, and Signal Processing Workshops (ICASSPW)*, pp. 1–5. IEEE, 2023.

Fabian Mentzer, David Minnen, Eirikur Agustsson, and Michael Tschannen. Finite scalar quantization: Vq-vae made simple. *arXiv preprint arXiv:2309.15505*, 2023.

Adam Paszke, Sam Gross, Francisco Massa, Adam Lerer, James Bradbury, Gregory Chanan, Trevor Killeen, Zeming Lin, Natalia Gimelshein, Luca Antiga, et al. Pytorch: An imperative style, high-performance deep learning library. *Advances in neural information processing systems*, 32, 2019.

Marc'Aurelio Ranzato, Sumit Chopra, Michael Auli, and Wojciech Zaremba. Sequence level training with recurrent neural networks. In *4th International Conference on Learning Representations (ICLR), May 2-4, 2016, Conference Track Proceedings*, 2016.

Ali Razavi, Aaron Van den Oord, and Oriol Vinyals. Generating diverse high-fidelity images with vq-vae-2. *Advances in neural information processing systems*, 32, 2019.

Danilo Jimenez Rezende and Fabio Viola. Taming vaes. *arXiv preprint arXiv:1810.00597*, 2018.

Olga Russakovsky, Jia Deng, Hao Su, Jonathan Krause, Sanjeev Satheesh, Sean Ma, Zhiheng Huang, Andrej Karpathy, Aditya Khosla, Michael Bernstein, Alexander C. Berg, and Li Fei-Fei. ImageNet Large Scale Visual Recognition Challenge. *International Journal of Computer Vision (IJCV)*, 115(3):211–252, 2015.

Myungseo Song, Jinyoung Choi, and Bohyung Han. Variable-rate deep image compression through spatially-adaptive feature transform. In *Proceedings of the IEEE/CVF International Conference on Computer Vision*, pp. 2380–2389, 2021.

Ilya Sutskever, Oriol Vinyals, and Quoc V Le. Sequence to sequence learning with neural networks. *Advances in neural information processing systems*, 27, 2014.

Yuhta Takida, Takashi Shibuya, Weihsiang Liao, Chieh-Hsin Lai, Junki Ohmura, Toshimitsu Uesaka, Naoki Murata, Shusuke Takahashi, Toshiyuki Kumakura, and Yuki Mitsufuji. Sq-vae: Variational bayes on discrete representation with self-annealed stochastic quantization. In *International Conference on Machine Learning*, pp. 20987–21012. PMLR, 2022.

Aaron Van Den Oord, Oriol Vinyals, et al. Neural discrete representation learning. *Advances in neural information processing systems*, 30, 2017.

Aäron van den Oord, Nal Kalchbrenner, and Koray Kavukcuoglu. Pixel recurrent neural networks. In *Proceedings of The 33rd International Conference on Machine Learning*, volume 48, pp. 1747–1756, New York, New York, USA, 20–22 Jun 2016. PMLR.

Benjamin Van Niekerk, Leanne Nortje, and Herman Kamper. Vector-quantized neural networks for acoustic unit discovery in the zerospeech 2020 challenge. *arXiv preprint arXiv:2005.09409*, 2020.

Tung-Long Vuong, Trung Le, He Zhao, Chuanxia Zheng, Mehrtash Harandi, Jianfei Cai, and Dinh Phung. Vector quantized wasserstein auto-encoder. *arXiv preprint arXiv:2302.05917*, 2023.

Zhou Wang, Alan C Bovik, Hamid R Sheikh, and Eero P Simoncelli. Image quality assessment: from error visibility to structural similarity. *IEEE transactions on image processing*, 13(4):600–612, 2004.

Ronald J Williams and David Zipser. A learning algorithm for continually running fully recurrent neural networks. *Neural computation*, 1(2):270–280, 1989.

Hanwei Wu and Markus Flierl. Vector quantization-based regularization for autoencoders. In *Proceedings of the AAAI Conference on Artificial Intelligence*, volume 34, pp. 6380–6387, 2020.

Jinbo Xing, Menghan Xia, Yuechen Zhang, Xiaodong Cun, Jue Wang, and Tien-Tsin Wong. Codetalker: Speech-driven 3d facial animation with discrete motion prior. In *Proceedings of the IEEE/CVF Conference on Computer Vision and Pattern Recognition*, pp. 12780–12790, 2023.

Dongchao Yang, Jianwei Yu, Helin Wang, Wen Wang, Chao Weng, Yuexian Zou, and Dong Yu. Diffsound: Discrete diffusion model for text-to-sound generation. *IEEE/ACM Transactions on Audio, Speech, and Language Processing*, 2023.

Fei Yang, Luis Herranz, Joost Van De Weijer, José A Iglesias Guitián, Antonio M López, and Mikhail G Mozerov. Variable rate deep image compression with modulated autoencoder. *IEEE Signal Processing Letters*, 27:331–335, 2020.

Jiahui Yu, Xin Li, Jing Yu Koh, Han Zhang, Ruoming Pang, James Qin, Alexander Ku, Yuanzhong Xu, Jason Baldridge, and Yonghui Wu. Vector-quantized image modeling with improved vqgan. In *International Conference on Learning Representations*, 2022.

Richard Zhang, Phillip Isola, Alexei A. Efros, Eli Shechtman, and Oliver Wang. The unreasonable effectiveness of deep features as a perceptual metric. In *Proceedings of the IEEE Conference on Computer Vision and Pattern Recognition (CVPR)*, June 2018.

Chuanxia Zheng and Andrea Vedaldi. Online clustered codebook. In *Proceedings of the IEEE/CVF International Conference on Computer Vision*, pp. 22798–22807, 2023.

Yongxin Zhu, Bocheng Li, Yifei Xin, and Linli Xu. Addressing representation collapse in vector quantized models with one linear layer. *arXiv preprint arXiv:2411.02038*, 2024.

A Appendix

A.1 Experiment Details

A.1.1 Architectures and Hyperparameters

The model architecture for this study is based on the conventional VQ-VAE framework outlined in the original VQ-VAE paper (Van Den Oord et al., 2017), and is implemented with reference to the VQ-VAE-2 (Razavi et al., 2019) implementation repositories[1][2][3] and an open-source VQ-VAE + PixelCNN implementation used for our unconditional prior experiments.[4] We also relied on open-source VQGAN resources, including pretrained generator/discriminator weights[5] and a PyTorch implementation[6] used for training and evaluation pipelines.

We are using the ConvResNets from the repositories. These networks consist of convolutional layers, transpose convolutional layers and ResBlocks. Experiments were conducted on two different computer setups: a server with 4 RTX 4090 GPUs and a machine with 2 RTX 3090 GPUs. PyTorch (Paszke et al., 2019), PyTorch Lightning (Falcon, 2019), and the AdamW (Loshchilov & Hutter, 2019) optimizer were used for model implementation and training. Evaluation metrics such as the Structural Similarity Index (SSIM) and the Frechet Inception Distance (rFID) were computed using implementations of pytorch-msssim [7] and pytorch-fid [8], respectively. The detailed model parameters are shown in Table 2. RAQs are constructed based on the described VQ-VAE parameters with additional consideration of each parameter.

Table 2: Architecture and hyperparameters for training VQ-VAE and RAQ models.

Method	Parameter	CIFAR10	CelebA	ImageNet
VQ-VAE (Van Den Oord et al., 2017)	Input size	32×32×3	$64 \times 64 \times 3$, $128 \times 128 \times 3$	224×224×3
	Latent layers	8×8	16×16, 32×32	56×56
	Hidden units	128	128	256
	Residual units	64	64	128
	# of ResBlock	2	2	2
	Original codebook size (K)	$2^4 \sim 2^{10}$	$2^5 \sim 2^{11}$	$2^7 \sim 2^{12}$
	Codebook dimension (d)	64	64	128
	β (Commit loss weight)	0.25	0.25	0.25
	Weight decay in EMA (γ)	0.99	0.99	0.99
	Batch size	128	128	32
	Optimizer	AdamW	AdamW	AdamW
	Learning rate	0.0005	0.0005	0.0005
	Max. training steps	195K	635.5K	961K
Model-based RAQ	Original codebook size (K)	64, 128	128, 256	512
	Adapted codebook size ($\widetilde{K}$)	$2^4 \sim 2^{10}$	$2^5 \sim 2^{11}$	$2^6 \sim 2^{12}$
	Max. DKM iteration	200	200	200
	Max. IKM iteration	5000	5000	5000
	τ of softmax	0.01	0.01	0.01
RAQ	Original codebook size (K)	64, 128	128, 256	512
	Adapted codebook size ($\widetilde{K}$)	$2^4 \sim 2^{10}$	$2^5 \sim 2^{11}$	$2^6 \sim 2^{12}$
	Max. Codebook size	1024	2048	4096
	Min. Codebook size	8	16	64
	Input size (Seq2Seq)	64	64	128
	Hidden size (Seq2Seq)	64	64	128
	# of recurrent layers (Seq2Seq)	2	2	2

A.1.2 Datasets and Preprocessing

For the **CIFAR10** dataset, the training set is preprocessed using a combination of random cropping and random horizontal flipping. Specifically, a random crop of size 32×32 with padding of 4 using

[1] https://github.com/mattiasxu/VQVAE-2
[2] https://github.com/rosinality/vq-vae-2-pytorch
[3] https://github.com/EugenHotaj/pytorch-generative
[4] https://github.com/KimRass/VQ-VAE-PixelCNN
[5] https://github.com/aa1234241/vqgan
[6] https://github.com/dome272/VQGAN-pytorch
[7] https://github.com/VainF/pytorch-msssim
[8] https://github.com/mseitzer/pytorch-fid

the 'reflect' padding mode is applied, followed by a random horizontal flip. The validation and test sets are processed by converting the images to tensors without further augmentation. For the **CelebA** dataset, the training set is preprocessed with a series of transformations. The images are resized and center cropped to 64×64 or 128×128, normalized, and subjected to random horizontal flipping. A similar preprocessing is applied to the validation set, while the test set is processed without augmentation. For the **ImageNet** dataset, the training set is preprocessed with a series of transformations. The images are resized to 256×256 and center cropped to 224×224, normalized, and subjected to random horizontal flipping. A similar preprocessing is applied to the validation set, while the test set is processed without augmentation. These datasets are loaded into PyTorch using the provided data modules, and the corresponding data loaders are configured with the specified batch sizes and learning rate for efficient training (described in Table 2). The datasets are used as input for training, validation, and testing of the VQ-VAE model.

A.2 Model-Based RAQ: Additional Details and Analyses

A.2.1 Codebook Clustering

In this subsection, we formalize codebook clustering for model-based RAQ and fix notation used by DKM. Given a set of the original codebook representations $\mathbf{e} = \{e_i\}_{i=1}^{K}$, we aim to partition the K codebook vectors into $\widetilde{K}(\leq K)$ codebook vectors $\tilde{\mathbf{e}} = \{\tilde{e}_i\}_{i=1}^{\widetilde{K}}$. Each codebook vector resides in a D-dimensional Euclidean space. Using the codebook assignment function $g(\cdot)$, then $g(e_i) = j$ means i-th given codebook assigned j-th clustered codebook. Our objective for codebook clustering is to minimize the discrepancy $\mathcal{L}$ between the given codebook $\mathbf{e}$ and clustered codebook $\tilde{\mathbf{e}}$:

$$\arg\min_{\tilde{\mathbf{e}},g} \mathcal{L}(\mathbf{e};\tilde{\mathbf{e}}) = \arg\min_{\tilde{\mathbf{e}},g} \sum_{i=1}^{\widetilde{K}} ||e_i - \tilde{e}_{g(e_i)}|| \tag{7}$$

with necessary conditions

$$g(e_i) = \arg\min_{j \in 1,2,\ldots,\widetilde{K}} ||e_i - \tilde{e}_j|| \,, \quad \tilde{e}_j = \frac{\sum_{i:g(e_i)=j} e_i}{N_j} \tag{8}$$

where N_j is the number of samples assigned to the codebook $\tilde{e}_j$.

A.2.2 Codebook Expansion (via IKM)

We now describe codebook expansion for model-based RAQ and the inverse-functional DKM (IKM) procedure used to synthesize a larger codebook from a trained one.

While k-means clustering is effective for compressing codebook vectors, it has algorithmic limitations when *adding* new codebook vectors. To address this, we introduce inverse-functional DKM (IKM), which increases the number of codebook vectors by approximating the distribution of a trained codebook. We measure distributional discrepancy via maximum mean discrepancy (MMD) between the base codebook and the clustered, synthesized codebook. MMD is a kernel-based two-sample statistic that quantifies distributional similarity (Gretton et al., 2012).

Given a trained base codebook $\mathbf{e}$ of size K, IKM generates an expanded codebook $\tilde{\mathbf{e}}$ of size $\widetilde{K} > K$ as follows:

- Initialize a d-dimensional adapted codebook vector $\tilde{\mathbf{e}} = \{\tilde{e}_i\}_{i=1}^{\widetilde{K}}$ as $\tilde{\mathbf{e}} \sim \mathcal{N}(0, d^{-\frac{1}{2}} \boldsymbol{I}_{\widetilde{K}})$
- Cluster $\tilde{\mathbf{e}}$ via the DKM process (equation 6): $g_{\text{DKM}}(\tilde{\mathbf{e}}) = \arg\min_{g_{\text{DKM}}(\tilde{\mathbf{e}})} \mathcal{L}_{\text{DKM}}(\tilde{\mathbf{e}}; g_{\text{DKM}}(\tilde{\mathbf{e}}))$.
- Calculate the MMD between the true original codebook $\mathbf{e}$ and the DKM clustered $g_{\text{DKM}}(\tilde{\mathbf{e}})$.
- Optimize $\tilde{\mathbf{e}}$ to minimize the MMD objective $\mathcal{L}_{\text{IKM}}(\mathbf{e};\tilde{\mathbf{e}}) = \text{MMD}(\mathbf{e}, g_{\text{DKM}}(\tilde{\mathbf{e}})) + \lambda||\tilde{\mathbf{e}}||^2$.

where λ is the regularization parameter controlling the strength of the L2 regularization term. The IKM process can be summarized as $\tilde{\mathbf{e}} = \arg\min_{\tilde{\mathbf{e}}} \mathcal{L}_{\text{IKM}}(\mathbf{e};\tilde{\mathbf{e}})$. Since DKM does not block gradient flow, we easily can update the codebook $\tilde{\mathbf{e}}$ using stochastic gradient descent (SGD) as $\tilde{\mathbf{e}} = \tilde{\mathbf{e}} - \eta \nabla \mathcal{L}_{\text{IKM}}(\mathbf{e},\tilde{\mathbf{e}})$.

A.2.3 Initialization Sensitivity in Expansion

We observe a marked degradation when increasing the codebook size ($\widetilde{K} > K$) under the clustering-only variant. Empirically, this is primarily driven by initialization in IKM: newly synthesized vectors may be placed far from the manifold spanned by the trained base codebook, making soft assignments unstable and prone to poor local minima. This yields higher run-to-run variance and lower reconstruction quality at large $\widetilde{K}$.

While our primary focus is the novelty and efficacy of the Seq2Seq-based RAQ, a systematic study of more robust initialization strategies for model-based RAQ remains promising future work.

A.2.4 Comparison to Clustering Baselines

We compare the model-based RAQ variant against standard clustering/compression baselines on a pre-trained VQ-VAE (trained on CelebA 64×64) using the base codebook ($K = 1024$). For each target adapted codebook size $\widetilde{K} \in \{512, 256, 128\}$, we adapt the codebook with:

- **DKM**: As described in our main paper.
- **k-means++**: An effective initialization method for the k-means clustering algorithm.
- **Gaussian Mixture Model (GMM)**: A probabilistic clustering method assuming data points come from a finite mixture of Gaussian distributions.
- **DKM + post-training**: Fine-tuning the original VQ model using the compressed codebook obtained from DKM.

Table 3: Comparison of codebook clustering methods for model-based RAQ. Metrics are PSNR↑ / SSIM↑ / Perplexity↑; mean over 4 seeds.

Method	Adapted codebook size $\widetilde{K}$			
	1024	512	256	128
DKM	26.41 / 0.8351 / 99.9	25.24 / 0.8078 / 52.3	24.37 / 0.7720 / 32.5	23.20 / 0.7415 / 20.0
k-means++	26.22 / 0.8400 / 60.8	25.28 / 0.8071 / 40.2	24.51 / 0.7872 / 29.4	23.38 / 0.7486 / 21.3
GMM	26.19 / 0.8350 / 62.4	25.22 / 0.8057 / 40.1	24.46 / 0.7814 / 30.0	23.51 / 0.7487 / 21.3
DKM + post-training	**28.39 / 0.8959 / 180.9**	**27.69 / 0.8842 / 95.0**	**26.97 / 0.8675 / 56.7**	**25.66 / 0.8309 / 28.6**

Table 3 indicate that basic clustering methods achieve similar codebook reduction performance. However, the differentiable nature of DKM uniquely enables efficient fine-tuning, substantially improving the compression performance within the same model architecture. Thus, while initial clustering performance differences are modest, the capability for post-training underscores the notable advantage and novelty of our proposed RAQ method.

A.2.5 Model Complexity

In this section, we provide a comparison of model complexity in terms of the total number of trainable parameters for our VQ-based models, both with and without our RAQ module. The following tables list parameter counts for the VQ-VAE and RAQ (our proposed method) variations on (i) CIFAR10 (Table 4), (ii) CelebA (Table 5), and (iii) ImageNet (Table 6).

As shown in the tables below, the addition of RAQ introduces a new Seq2Seq component to facilitate codebook adaptation, resulting in a modest increase in the number of parameters:

- In **VQ-VAE**, whose total parameter count is on the order of a few hundred thousand, the RAQ overhead typically adds $\sim$ 200K+ parameters (e.g., for CIFAR10, the total parameter count increases from about 468K to 732K for $K = 128$).
- In **stage-1 VQGAN**, which already has tens of millions of parameters, the additional parameters introduced by RAQ are less than 1% of the total. For instance, the total grows from 72.0M to approximately 72.6M—a practically negligible difference in large-scale settings.

These observations demonstrate that RAQ remains practical for a variety of model scales and does not incur substantial overhead, even when applied to deeper architectures.

Table 4: Number of parameters for training VQ-VAE and RAQ models on the CIFAR10 dataset.

Method	# params				
	Encoder	Decoder	Quantizer	Seq2Seq	Total
VQ-VAE ($K = 1024$)	196.3K	262K	65.5K	-	525K
VQ-VAE ($K = 512$)	196.3K	262K	32.8K	-	492K
VQ-VAE ($K = 256$)	196.3K	262K	16.4K	-	476K
VQ-VAE ($K = 128$)	196.3K	262K	8.2K	-	468K
VQ-VAE ($K = 64$)	196.3K	262K	4.1K	-	463K
VQ-VAE ($K = 32$)	196.3K	262K	2.0K	-	461K
VQ-VAE ($K = 16$)	196.3K	262K	1.0K	-	460K
RAQ ($K = 128$)	196.3K	262K	8.2K	263.7K	732K
RAQ ($K = 64$)	196.3K	262K	4.1K	263.7K	728K

Table 5: Number of parameters for training VQ-VAE and RAQ models on the CelebA dataset.

Method	**# params**				
	Encoder	Decoder	Quantizer	Seq2Seq	Total
VQ-VAE ($K = 2048$)	196.3K	262K	131K	-	590K
VQ-VAE ($K = 1024$)	196.3K	262K	65.5K	-	525K
VQ-VAE ($K = 512$)	196.3K	262K	32.8K	-	492K
VQ-VAE ($K = 256$)	196.3K	262K	16.4K	-	476K
VQ-VAE ($K = 128$)	196.3K	262K	8.2K	-	468K
VQ-VAE ($K = 64$)	196.3K	262K	4.1K	-	463K
VQ-VAE ($K = 32$)	196.3K	262K	2.0K	-	461K
RAQ ($K = 256$)	196.3K	262K	16.4K	263.7K	740K
RAQ ($K = 128$)	196.3K	262K	8.2K	263.7K	732K

Table 6: Number of parameters for training stage-1 VQGAN and RAQ models on the ImageNet dataset.

Method	**# params**		
	Quantizer	Seq2Seq	Total
VQGAN ($K = 512$)	65.5K	-	72.0M
VQGAN ($K = 256$)	32.8K	-	72.0M
VQGAN ($K = 128$)	16.4K	-	72.0M
VQGAN ($K = 64$)	8.2K	-	72.0M
VQGAN ($K = 32$)	4.1K	-	71.9M
RAQ ($K = 128$)	16.4K	610K	72.6M

A.2.6 TRAINING/INFERENCE TIME

Setup All timings were measured on a single NVIDIA RTX 3090 with batch size 128. We report per-epoch wall-clock time. We compare a single RAQ model (K=256) against multiple fixed-rate VQ baselines ($K \in \{64, 256, 1024\}$) and the model-based RAQ.

Training Time As expected, adding the Seq2Seq adapter increases per-epoch time versus a single fixed-rate VQ; however, when multiple bitrates are required, one RAQ model replaces several separately trained VQs, reducing total training and maintenance cost.

Table 7: Training time per epoch on the CelebA train set using an NVIDIA RTX 3090 GPU.

Method	K	Training time per epoch (s)	# params
VQ-VAE / Model-based RAQ	64	18.09 ± 0.256	463K
VQ-VAE / Model-based RAQ	256	18.43 ± 0.10	476K
VQ-VAE / Model-based RAQ	1024	21.64 ± 0.11	525K
RAQ	256	514.97 ± 8.17	740K

Inference Time We consider two deployment regimes: (i) a *pessimistic* setting that regenerates the adapted codebook for *every* mini-batch (upper bound on cost), and (ii) a *cached* setting that adapts the codebook *once per target rate* $\widetilde{K}$ and reuses it thereafter (realistic case).

Table 8: Inference time per epoch on CelebA (test set) when *regenerating per mini-batch*.

Method	$\widetilde{K}$	Inference time per epoch (s)
VQ-VAE ($K = 64$)	–	1.86 ± 0.10
VQ-VAE ($K = 256$)	–	1.91 ± 0.12
VQ-VAE ($K = 1024$)	–	1.86 ± 0.09
Model-based RAQ ($K = 256$)	64	1.98 ± 0.09
RAQ ($K = 256$)	64	3.05 ± 0.11
Model-based RAQ ($K = 256$)	1024	70.91 ± 11.82
RAQ ($K = 256$)	1024	33.21 ± 0.27

One-time Codebook Adaptation Latency To reflect practical use, we additionally measure the one-time latency to adapt and cache a codebook for a given $\widetilde{K}$; subsequent batches reuse this codebook at no extra cost. The added latency is on the order of 10-140 ms.

Table 9: One-time adaptation latency per target rate (cached at inference).

$\widetilde{K}$	Latency (ms)
64	9.67 ± 10.34
128	18.08 ± 9.32
256	36.00 ± 9.49
512	71.63 ± 10.99
1024	143.94 ± 12.63

Summary Table 8 should be interpreted as an upper bound (regenerate-per-batch). In realistic deployments (adapting once per $\widetilde{K}$ and caching) the extra latency (Table 9) is negligible, while a single RAQ model still replaces multiple fixed-rate VQs in storage and operational complexity.

A.3 Additional Experiments

A.3.1 Stage-2 Compatibility with Autoregressive Priors

In our end-to-end setups, the stage-2 VQ model is an autoregressive Transformer prior trained on sequences of VQ code indices produced by the stage-1 VQ encoder. Rather than refining pixels directly, it models the distribution of latent token sequences and generates new index sequences that the VQ decoder then maps back to images. This factorization enables us to pair RAQ-adapted latents

with a fixed stage-2 prior across multiple target rates $\widetilde{K}$ without the need for retraining separate stage-1 models.

RAQ-VAE denotes a standard VQ-VAE whose stage-1 quantizer is augmented with our Seq2Seq codebook adaptation module. *RAQGAN* analogously augments a stage-1 VQGAN (generator and discriminator) with the same RAQ module, leaving the adversarial training pipeline unchanged.

RAQ-VAE with PixelCNN First, we evaluated the performance of unconditional image generation by combining the trained Stage-1 autoencoders (VQ-VAE and RAQ-VAE) with a PixelCNN decoder that was trained on the Fashion-MNIST dataset. For each codebook size, we generated 10,000 samples via categorical sampling with a temperature of 1.0, and reported both the Inception Score (IS) and the Fréchet Inception Distance (FID), which are the most widely adopted metrics for generative modelling.

Table 10: Evaluation of unconditional image generation. PixelCNN with stage-1 VQ-VAE encoder (*top*) and single stage-1 RAQ-VAE encoder (*bottom*).

Method	$\widetilde{K}$	FID ↓	IS ↑
VQ-VAE (K=256) + PixelCNN	–	48.88	4.04
VQ-VAE (K=128) + PixelCNN	–	53.46	3.95
VQ-VAE (K=64) + PixelCNN	–	53.69	3.95
VQ-VAE (K=32) + PixelCNN	–	54.58	4.14
VQ-VAE (K=16) + PixelCNN	–	58.53	3.92
RAQ (K=64) + PixelCNN	256	47.96	4.09
	128	50.81	4.08
	64	51.24	4.06
	32	52.43	3.98
	16	58.47	3.96

As shown in Table 10, RAQ-VAE combined with PixelCNN achieves competitive, and in some cases slightly improved, FID and IS values across all tested codebook sizes compared to baseline VQ-VAE. This demonstrates that the expressivity of the RAQ-adapted latent variables is well preserved for synthesis purposes.

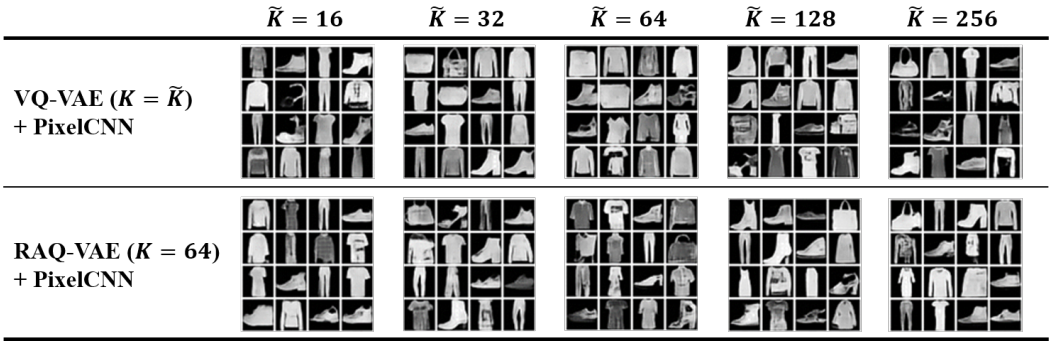

Figure 4: Unconditional samples with a PixelCNN prior. Top: VQ-VAE baselines (K=$\widetilde{K}$). Bottom: one RAQ-VAE (K=64) with $\widetilde{K}$.

Qualitatively, both fixed-rate VQ-VAE and the single RAQ-VAE produce diverse, coherent samples across the rates. RAQ maintains comparable visual fidelity while varying $\widetilde{K}$ without retraining the stage-1 model.

RAQGAN with Transformer Next, to further evaluate conditional image generation, we integrated VQGAN and RAQGAN stage-1 models with a transformer-based autoregressive prior (minGPT) on the Oxford Flowers102 dataset. We fine-tuned each model (with pretrained encoder, generator, and discriminator) on the Flowers102 train dataset across various codebook sizes and generated 6149 half-conditional test samples.

Table 11: Evaluation of conditional image generation (temperature 1.0, top-k sampling of $k = 100$). MinGPT with stage-1 VQGAN generator (*top*) and single stage-1 RAQGAN generator (*bottom*).

Method	$\widetilde{K}$	FID ↓
VQGAN (K=1024) + minGPT	–	35.67
VQGAN (K=512) + minGPT	–	40.13
VQGAN (K=256) + minGPT	–	38.47
RAQ (K=512) + minGPT	1024	34.00
	512	33.47
	256	35.47

In Table 11, the results demonstrate that RAQGAN can be effectively combined with an autoregressive transformer prior, yielding performance on par with or superior to standard VQGAN-based models. Furthermore, our results demonstrate that a single RAQ-based model can flexibly support a wide range of adapted codebook sizes with consistently strong generative quality, unlike conventional VQGAN-Transformer approaches that require training separate VQGANs for each bitrate or target rate. Notably, RAQ-adapted latents remain fully compatible with stage-2 autoregressive models, allowing seamless end-to-end synthesis at arbitrary rates. This property is especially beneficial in practical deployment scenarios, where resource constraints or bandwidth conditions may change dynamically, as it enables flexible adaptation to different rates without retraining or model switching.

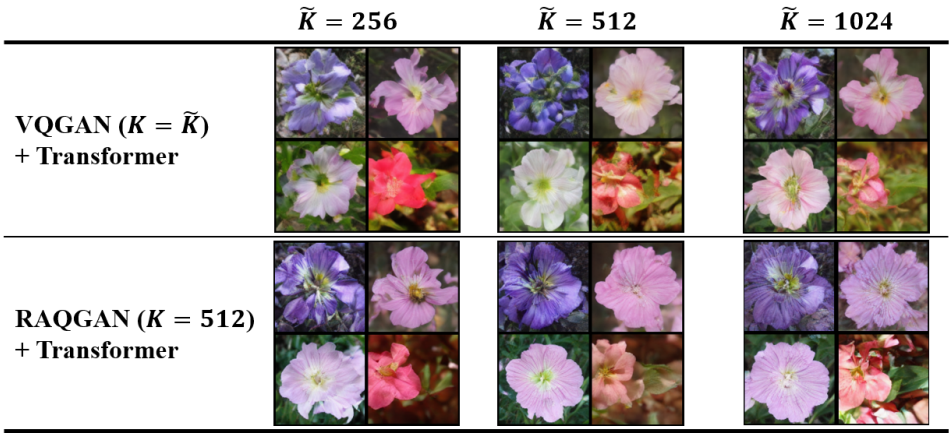

Figure 5: Conditional samples with Transformer (minGPT) on Flowers102 dataset. Top: VQGAN baselines (K=$\widetilde{K}$). Bottom: one RAQGAN (K=512) with $\widetilde{K}$.

Qualitatively, both VQGAN and the single RAQGAN yield diverse, class-consistent samples. RAQGAN maintains comparable visual quality while varying $\widetilde{K}$ without retraining the stage-1 model.

Across both priors, these small-scale studies suggest that RAQ-adapted latent variables are compatible with stage-2 VQ models over a range of $\widetilde{K}$ and can be paired with off-the-shelf priors without additional stage-1 retraining. While a broader evaluation is left to future work, the evidence here supports straightforward end-to-end use of one stage-1 model under changing bitrate constraints.

A.3.2 Effectiveness of Cross-Forcing

We performed an ablation study to analyze the impact of our *cross-forcing* training strategy on the stability and fidelity of codebook generation. Using a base RAQ model with an original codebook size $K = 128$ on the CelebA dataset, we compared two variants: (1) *RAQ-w/o-CF* without cross-forcing, and (2) *RAQ-w/-CF* with cross-forcing. Table 12 shows the reconstruction metrics (MSE, PSNR, rFID, and SSIM) for different adapted codebook sizes $\widetilde{K} \in \{32, 64, 128, 256, 512, 1024, 2048\}$. We find that *RAQ-w/-CF* gives significantly better performance than *RAQ-w/o-CF* when $\widetilde{K} > K$, leading to up to 4.9% improvement in rFID and noticeable gains in PSNR and SSIM. In contrast, for smaller or equal codebook sizes ($\widetilde{K} \leq K$), *RAQ-w-CF* sometimes

Table 12: Reconstruction performance of RAQ ($K = 128$) **with** or **without** cross-forcing on the CelebA test dataset

Method	$\widetilde{K}$	MSE ($\times 10^3$) ↓	PSNR ↑	rFID ↓	SSIM ↑
RAQ-**w/**-CF	2048 (↑)	**1.618±0.016**	**27.91±0.04**	**22.64±0.76**	**0.8810±0.0013**
	1024 (↑)	**1.794±0.027**	**27.47±0.07**	**24.67±0.80**	**0.8710±0.0016**
	512 (↑)	**2.042±0.021**	**26.90±0.05**	**26.90±0.04**	**0.8589±0.0044**
	256 (↑)	**2.412±0.101**	**26.18±0.18**	**30.81±1.59**	0.8391±0.0125
	128 (-)	2.801±0.039	25.53±0.06	36.30±1.12	0.8209±0.0072
	64 (↓)	3.895±0.095	24.10±0.11	47.63±5.82	0.7892±0.0067
	32 (↓)	**5.357±0.630**	**22.74±0.54**	**62.39±3.76**	**0.7414±0.0304**
RAQ-**w/o**-CF	2048 (↑)	1.661±0.056	27.80±0.14	23.58±0.26	0.8789±0.0030
	1024 (↑)	1.815±0.050	27.42±0.12	25.46±0.26	0.8705±0.0024
	512 (↑)	2.068±0.059	26.85±0.12	27.81±0.42	0.8567±0.0046
	256 (↑)	2.449±0.052	26.12±0.09	32.32±1.20	**0.8407±0.0031**
	128 (-)	**2.779±0.015**	**25.57±0.02**	**36.08±0.98**	**0.8261±0.0019**
	64 (↓)	**3.860±0.237**	**24.15±0.26**	**45.13±2.79**	**0.7942±0.0154**
	32 (↓)	6.289±0.709	22.04±0.47	72.85±16.69	0.7338±0.0225

underperforms its counterpart by a small margin. We hypothesize that cross-forcing is specifically designed to stabilize the generation of *larger* adapted codebooks (up to twice the original size), which can result in a slight tradeoff when quantizing at or below the baseline codebook size.

A.3.3 SEQ2SEQ MODEL SIZE

Regarding the sensitivity of our RAQ to the Seq2Seq model size, we conducted additional experiments. Using our RAQ framework applied to a VQ-VAE-2 (Razavi et al., 2019) baseline on the CelebA (128×128) dataset with an original codebook size of $K = 256$, we compared two configurations:

- **RAQ with 2 LSTM layers:** This configuration uses approximately 528K parameters in the Seq2Seq model (about 10.78% of the total model parameters).
- **RAQ with 4 LSTM layers:** Here, the Seq2Seq model's parameter count increases to approximately 1.06M (about 19.63% of the total model parameters).

Table 13: RAQ performance with different layer configurations on varying codebook sizes. We controlled all other variables over four random seeds (only values significantly outside the confidence interval are bolded).

Method	$\widetilde{K}$	PSNR	LPIPS	Perplexity (%)
RAQ, 2 layers	2048	33.26	0.1097	22.71
	1024	32.77	0.1171	23.41
	512	32.24	0.1256	26.10
	256	31.33	0.1439	26.18
	128	30.39	0.1663	30.21
	64	**28.76**	0.2009	37.89
RAQ, 4 layers	2048	33.16	0.1052	22.53
	1024	32.76	**0.1107**	24.28
	512	32.17	**0.1192**	26.54
	256	**31.49**	**0.1325**	25.05
	128	30.40	**0.1548**	31.36
	64	27.79	**0.2162**	35.45

The results show that increasing the LSTM layers from 2 to 4 yields only marginal improvements (e.g., a slight improvement in LPIPS) despite nearly doubling the parameter count. These findings indicate that our compact LSTM-based design achieves an appropriate balance between computational efficiency and performance within our current framework. We also note that if the baseline

VQ model were considerably larger (for example, using a ViT-based encoder/decoder), the relative impact of the Seq2Seq model's size might be reduced, and exploring larger architectures could be more promising.

A.3.4 CODEBOOK SIZE SWITCHING WITHIN A SEQUENCE

To evaluate the stability of our RAQ scheme when switching between codebook sizes within a sequence, we conducted additional experiments on the Kodak dataset. We used a VQ-VAE-2 model trained with RAQ (original codebook size $K = 256$) on ImageNet (256×256) and varied the adapted codebook sizes for both the bottom- and top-level latent maps during inference. Table 14 summarizes the PSNR, SSIM, and LPIPS metrics under all combinations of bottom- and top-level codebook sizes.

Table 14: Performance when switching between codebook sizes for top and bottom latent codes on Kodak dataset). The input to the model is 768x512 images of Kodak dataset that is compressed to quantized latent maps of size 192×128 and 96×64 for the bottom and top levels, respectively.

Bottom $\widetilde{K}$	Top $\widetilde{K}$	PSNR	SSIM	LPIPS
4096	4096	30.24	0.9739	0.10698
4096	1024	30.21	0.9735	0.10850
1024	4096	29.80	0.9706	0.11491
1024	1024	29.78	0.9701	0.11628
1024	256	29.70	0.9691	0.11930
256	1024	29.00	0.9639	0.13077
256	256	28.96	0.9631	0.13298
256	64	28.79	0.9607	0.13941
64	256	27.98	0.9528	0.15973
64	64	27.85	0.9506	0.16575

These results confirm that switching codebook sizes within a latent sequence does not degrade reconstruction stability. Prior work reports that the top-level code captures global structure while the bottom-level code encodes local details (Razavi et al., 2019); our findings further reveal that the bottom-level codebook size exerts a stronger influence on reconstruction quality.

A.3.5 MODEL-BASED RAQ

Rate Reduction As analyzed in Section 5.2, RAQ generally outperforms model-based RAQ, but some rate-reduction results on CIFAR10 show that model-based RAQ performs much more stably than in the codebook increasing task. This indicates that simply clustering codebook vectors, without additional neural models like Seq2Seq, can achieve remarkable performance. In Table 15, the performance via codebook clustering was evaluated with different original/adapted codebook sizes K: 1024 / $\widetilde{K}$: 512, 256, 128 on CIFAR10 and K: 2048 / $\widetilde{K}$: 1024, 512, 256, 128 on CelebA. The conventional VQ-VAE preserved as many codebooks in the original codebook as in the adapted codebook, while randomly codebook-selected VQ-VAE results remained meaningless. Model-based RAQ adopted this baseline VQ-VAE model and performed clustering on the adapted codebook. Model-based RAQ shows a substantial performance difference in terms of reconstructed image distortion and codebook usage compared to randomly codebook-selected VQ-VAE. Even when evaluating absolute performance, it is intuitive that online codebook representation via model-based RAQ provides some performance guarantees.

Rate Expansion In our proposed RAQ scenario, increasing the codebook size beyond the base size is a more demanding and crucial task than reducing it. The crucial step in building RAQ is to achieve higher rates from a fixed model architecture and compression rate, ensuring usability. Therefore, the codebook increasing task was the main challenge. The Seq2Seq decoding algorithm based on cross-forcing is designed with this intention. In Figure 2, the codebook generation performance was evaluated with different original/adapted codebook sizes K: 64, 128 / $\widetilde{K}$: 64, 128, 256, 512, 1024 on CIFAR10 and K: 128, 256 / $\widetilde{K}$: 128, 256, 512, 1024, 2048 on CelebA datasets. RAQ outperforms model-based RAQ in the rate-increasing task and partially outperforms conventional

Table 15: Reconstruction performances of model-based RAQ for **rate-reduction task** according to adapted codebook size $\widetilde{K}$.

Method	$\widetilde{K}$	**CIFAR10** ($K = 1024$) PSNR ↑	rFID ↓	Perplexity ↑
VQ-VAE (baseline model)	-	25.48	51.90	708.60
VQ-VAE (random select)	512	24.35	63.67	**289.29**
	256	22.81	78.00	111.77
	128	20.87	93.57	48.87
Model-based RAQ	512	**24.62**	**55.78**	285.68
	256	**23.81**	**62.53**	**134.54**
	128	**23.07**	**69.45**	**73.17**
Method	$\widetilde{K}$	**CelebA** ($K = 2048$) PSNR ↑	rFID ↓	Perplexity ↑
VQ-VAE (baseline model)	-	28.26	22.89	273.47
VQ-VAE (random select)	1024	24.02	38.92	**103.50**
	512	18.99	71.64	49.59
	256	23.54	115.12	27.86
Model-based RAQ	1024	**26.40**	**31.37**	102.36
	512	**25.24**	**39.07**	**53.45**
	256	**24.36**	**45.54**	**32.86**

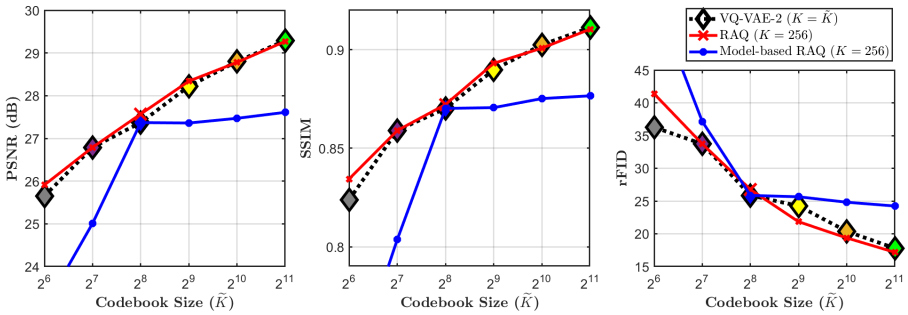

Figure 6: **Reconstruction performance** at different rates (adapted codebook sizes) evaluated on CelebA (64×64) test set. In the graph, the black VQ-VAE-2s (Razavi et al., 2019) are separate models trained on each codebook size, while the RAQs are one model per line.

VQ-VAE trained on the same codebook size ($K = \widetilde{K}$). This effect is particularly pronounced on CelebA. However, increasing the difference between the original and adapted codebook sizes leads to a degradation of RAQ performance. This effect is more dramatic for model-based RAQ due to its algorithmic limitations, making its performance less stable at high rates. Improving the performance of model-based RAQ, such as modifying the initialization of the codebook vector, remains a limitation.

A.3.6 Quantitative Results

VQ-VAE In Table 16 and 17, we present additional quantitative results for the reconstruction on CIFAR10 and CelebA datasets. The error indicates a 95.45% confidence interval based on 4 runs with different training seeds.

VQ-VAE-2 Figure 6 shows the reconstruction performance using VQ-VAE-2 as the baseline model.

Table 16: **Reconstruction performance** on CIFAR10 dataset. The 95.45% confidence interval is provided based on 4 runs with different training seeds.

Method	Bit Rate	Codebook Usability		Distortion	Perceptual Similarity	
	$\widetilde{K}$	Usage	Perplexity	PSNR	rFID	SSIM
VQ-VAE ($K = \widetilde{K}$)	1024	972.66±2.97	708.60±7.04	25.48±0.02	51.90±0.51	0.8648±0.0005
VQ-VAE ($K = \widetilde{K}$)	512	507.52±0.51	377.08±5.92	24.94±0.01	56.65±0.91	0.8490±0.0003
VQ-VAE ($K = \widetilde{K}$)	256	256±0	204.43±4.36	24.43±0.02	61.40±0.78	0.8310±0.0006
VQ-VAE ($K = \widetilde{K}$)	128	128±0	106.44±1.54	23.85±0.01	66.70±1.12	0.8096±0.0009
VQ-VAE ($K = \widetilde{K}$)	64	64±0	55.64±0.27	23.24±0.01	74.00±1.64	0.7849±0.0009
VQ-VAE ($K = \widetilde{K}$)	32	32±0	29.25±0.13	22.53±0.02	81.68±1.01	0.7545±0.0009
VQ-VAE ($K = \widetilde{K}$)	16	16±0	15.01±0.21	21.76±0.01	89.75±0.83	0.7156±0.0024
VQ-VAE ($K = 1024$) (random select)	1024	972.66±2.97	708.60±7.04	25.48±0.02	51.90±0.51	0.8648±0.0005
	512	498.38±1.85	289.29±16.67	24.35±0.11	63.67±2.49	0.8305±0.0056
	256	253.01±0.66	111.77±21.53	22.81±0.38	78.00±5.07	0.7822±0.0100
	128	127.34±0.33	48.87±11.31	20.87±0.73	93.57±9.87	0.7254±0.0235
	64	64±0	24.31±5.26	19.46±0.98	109.90±14.20	0.6720±0.0309
	32	32±0	13.50±1.45	17.76±1.12	126.57±15.89	0.6102±0.0350
RAQ ($K = 128$)	1024	979.16±3.72	738.48±7.39	25.18±0.03	54.65±0.99	0.8520±0.0007
	512	507.47±0.85	387.18±6.87	24.82±0.02	57.57±0.95	0.8417±0.0005
	256	256±0	207.78±12.13	24.34±0.02	61.76±1.22	0.8274±0.0008
	128	128±0	107.77±0.58	23.91±0.0	65.37±0.68	0.8132±0.0011
	64	64±0	55.59±1.81	22.87±0.04	77.49±2.39	0.7770±0.0036
	32	32±0	27.77±2.03	21.85±0.15	89.38±4.33	0.7356±0.0064
	16	16±0	14.84±0.74	20.82±0.09	98.93±4.64	0.6918±0.0033
Model-based RAQ ($K = 128$)	1024	744.36±18.74	395.23±2.77	24.15±0.03	63.88±1.26	0.8213±0.0014
	512	430.06±11.58	256.23±7.50	24.04±0.03	64.74±0.96	0.8177±0.0012
	256	244.61±3.13	185.02±3.31	23.93±0.01	65.65±1.12	0.8139±0.0010
	128	128±0	106.44±1.54	23.85±0.01	66.70±1.12	0.8096±0.0009
	64	64±0	49.55±1.29	22.85±0.55	72.61±0.77	0.7780±0.0013
	32	32±0	25.65±0.76	21.88±0.75	82.12±1.74	0.7405±0.0046
	16	16±0	13.79±0.06	20.89±0.04	95.03±0.34	0.6972±0.0010
RAQ ($K = 64$)	1024	972.14±6.49	725.55±10.90	25.04±0.01	55.34±1.48	0.8487±0.0012
	512	506.38±1.23	382.43±10.58	24.70±0.02	57.91±1.42	0.8387±0.0011
	256	255.52±0.48	196.17±9.95	24.25±0.02	61.96±1.00	0.8245±0.0012
	128	128±0	109.65±3.50	23.71±0.01	66.89±1.07	0.8071±0.0014
	64	64±0	56.31±0.46	23.23±0.01	71.17±1.17	0.7897±0.0013
	32	32±0	29.62±0.66	21.84±0.09	90.04±1.44	0.7350±0.0038
	16	16±0	15.11±0.67	20.79±0.18	104.86±5.91	0.6918±0.0084
Model-based RAQ ($K = 64$)	1024	706.20±115.18	345.50±107.06	23.65±0.13	70.30±2.02	0.8013±0.0051
	512	428.39±12.29	231.41±14.64	23.55±0.04	71.01±1.38	0.7988±0.0005
	256	233.75±4.63	140.19±2.82	23.39±0.05	71.72±1.43	0.7935±0.0012
	128	125.07±1.58	101.16±16.04	23.32±0.05	72.68±1.47	0.7901±0.0008
	64	64±0	55.64±0.27	23.24±0.01	74.00±1.64	0.7849±0.0009
	32	32±0	26.21±0.95	22.07±0.13	81.61±2.26	0.7569±0.0014
	16	16±0	13.59±0.85	20.88±0.23	92.84±3.30	0.7004±0.0063

Table 17: **Reconstruction performance** on CelebA dataset. The 95.45% confidence interval is provided based on 4 runs with different training seeds.

Method	Bit Rate	Codebook Usability		Distortion	Perceptual Similarity	
	$\widetilde{K}$	Usage	Perplexity	PSNR	rFID	SSIM
VQ-VAE ($K = \widetilde{K}$)	2048	779.07±8.35	273.47±6.86	28.26±0.03	22.89±0.71	0.8890±0.0027
VQ-VAE ($K = \widetilde{K}$)	1024	456.86±3.53	160.35±2.73	27.73±0.05	26.67±1.43	0.8763±0.0029
VQ-VAE ($K = \widetilde{K}$)	512	259.59±3.99	95.09±1.28	27.11±0.01	29.77±0.95	0.8636±0.0022
VQ-VAE ($K = \widetilde{K}$)	256	144.44±2.49	57.86±0.91	26.46±0.03	31.53±1.01	0.8481±0.0009
VQ-VAE ($K = \widetilde{K}$)	128	80.26±0.99	34.98±0.39	25.72±0.04	36.25±0.98	0.8279±0.0027
VQ-VAE ($K = \widetilde{K}$)	64	44.94±1.03	20.04±0.37	24.78±0.03	41.22±0.77	0.7986±0.0037
VQ-VAE ($K = \widetilde{K}$)	32	25.48±0.69	12.69±0.31	23.76±0.06	46.56±1.97	0.7660±0.0032
VQ-VAE ($K = 2048$) (random select)	2048	779.07±8.35	273.47±6.86	28.26±0.03	22.89±0.71	0.8890±0.0027
	1024	384.31±6.76	103.50±3.28	24.02±1.10	38.92±3.27	0.7963±0.0201
	512	210.69±9.23	49.59±4.54	18.99±1.40	71.64±8.27	0.7037±0.0221
	256	115.33±7.73	27.86±3.39	16.33±0.61	115.12±11.93	0.6353±0.0173
RAQ ($K = 256$)	2048	885.53±6.76	347.99±5.17	27.96±0.14	23.02±0.33	0.8858±0.0033
	1024	490.86±4.98	187.33±10.37	27.51±0.13	25.08±0.23	0.8758±0.0036
	512	275.84±1.72	104.61±5.00	26.95±0.086	27.96±0.49	0.8637±0.0045
	256	144.79±1.21	52.63±0.28	26.29±0.054	32.34±0.86	0.8463±0.0030
	128	80.21±4.27	32.23±3.87	25.13±0.26	39.67±2.29	0.8162±0.0071
	64	42.93±1.61	20.85±1.22	24.09±0.21	51.57±6.66	0.7912±0.0094
	32	22.76±1.57	12.32±0.91	22.62±0.27	69.65±9.49	0.7479±0.0129
Model-based RAQ ($K = 256$)	2048	704.17±108.04	117.53±33.57	26.54±0.10	30.34±1.39	0.8507±0.0041
	1024	460.77±26.98	134.48±11.26	26.59±0.06	30.49±1.10	0.8509±0.0021
	512	279.53±9.48	100.64±8.94	26.40±0.08	30.95±0.98	0.8488±0.0017
	256	144.44±2.49	57.86±0.91	26.46±0.03	31.53±1.01	0.8481±0.0009
	128	75.31±3.09	25.05±1.95	24.44±0.25	38.95±2.91	0.7890±0.0141
	64	41.66±1.22	14.73±0.56	22.85±0.36	48.96±1.13	0.7391±0.0192
	32	22.96±0.90	10.16±0.95	21.81±0.45	62.46±0.00	0.7077±0.0195
RAQ ($K = 128$)	2048	891.13±7.11	345.25±5.15	27.91±0.04	22.64±0.76	0.8810±0.0013
	1024	490.15±14.39	176.71±6.19	27.47±0.07	24.67±0.80	0.8710±0.0016
	512	272.60±2.08	96.87±2.68	26.90±0.05	26.90±0.04	0.8589±0.0044
	256	152.65±2.45	60.90±2.18	26.18±0.18	30.81±1.59	0.8391±0.0125
	128	79.17±0.93	31.36±0.77	25.53±0.06	36.30±1.12	0.8209±0.0072
	64	42.71±1.66	19.78±2.31	24.10±0.11	47.63±5.82	0.7892±0.0067
	32	22.42±1.92	11.43±2.14	22.74±0.54	62.39±3.76	0.7414±0.0304
Model-based RAQ ($K = 128$)	2048	350.02±100.57	64.87±21.22	22.77±0.78	52.37±10.94	0.7463±0.0347
	1024	432.15±45.80	102.79±17.34	25.57±0.19	35.62±1.46	0.8296±0.0062
	512	262.78±29.47	75.63±12.04	25.50±0.29	36.82±0.73	0.8265±0.0026
	256	153.16±5.46	53.22±4.62	25.42±0.28	36.78±1.27	0.8285±0.0022
	128	80.26±0.99	34.98±0.39	25.72±0.04	36.25±0.98	0.8279±0.0027
	64	41.88±0.72	16.70±0.43	23.63±0.16	47.09±4.09	0.7736±0.0080
	32	23.31±0.89	9.56±0.77	21.64±0.13	64.85±6.92	0.7037±0.0102

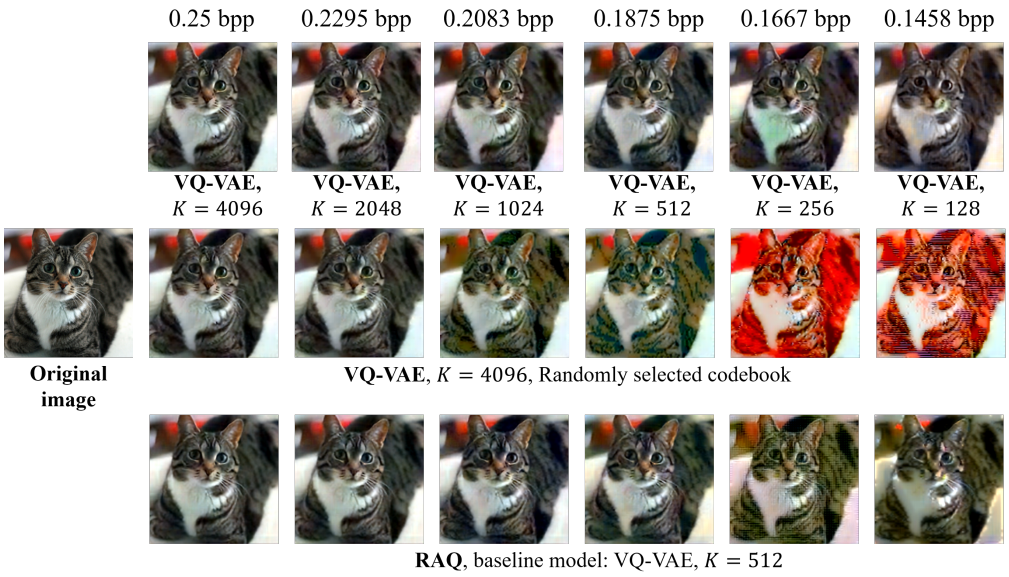

Figure 7: **Qualitative comparison** on ImageNet (256×256) at different compression rates. **Top row**: Fixed-rate VQ-VAEs trained separately at each rate. **Middle row**: A single VQ-VAE ($K = 4096$) with randomly selected codebooks. **Bottom row**: Our RAQ with VQ-VAE ($K = 512$) with adapting the codebook size.

A.3.7 Additional Qualitative Results

For our qualitative evaluation, We first compare a single RAQ-based model against multiple VQ-VAEs trained at different rates (0.1458 bpp to 0.25 bpp) on ImageNet (256×256). As illustrated in Figure 7, each fixed-rate VQ-VAE (top row) shows a progressive decline in image quality as the rate decreases, consistent with the quantitative evaluation. Unlike RAQ-based reconstruction, randomly selecting codebooks from a single VQ-VAE trained at $K = 4096$ (middle row) results in color distortions and inconsistent hues, especially at 0.1667 bpp. Despite retaining the basic structure, the mismatched usage of codebooks still produces unnatural appearances. By contrast, our RAQ-based VQ-VAE (bottom row), trained at a low-rate base codebook of 0.1875 bpp (roughly $K = 512$), effectively preserves high-level semantic features and color fidelity using only a single model. Notably, it recovers finer details (e.g., the cat's whiskers) far better than models relying on randomly selected codebooks. Although image quality declines slightly at the lowest bpp, largely due to the limited capacity of the baseline VQ-VAE, this issue can be mitigated by using more advanced VQ architectures or refining training procedures. Training RAQ with a smaller original codebook size K can also help reduce performance degradation at lower rates.

We conducted additional experiments using the VQ-VAE-2 model (Razavi et al., 2019) with an original codebook size of $K = 512$. To enhance perceptual quality, we incorporated the LPIPS loss (Zhang et al., 2018) into the training objective and trained the model on the ImageNet dataset at a resolution of 256×256. The reconstruction task involved reconstructing 24 high-quality images from the Kodak dataset (Kodak, 1993), each with a resolution of 768×512. For codebook adaptation, we adjusted the codebook size to $\widetilde{K} \in \{4096, 1024, 256, 64\}$ using our RAQ framework. The qualitative results are illustrated in Figure 8. Contrary to Figure 7, where reducing the codebook size in a less complex VQ-VAE model led to noticeable performance degradation, our RAQ-based VQ-VAE-2 demonstrated robust performance across various codebook sizes. Specifically, even as the codebook size decreased, the RAQ-based VQ-VAE-2 model effectively preserved image quality at higher resolutions. These results indicate that increasing the model complexity and refining the training methodology significantly enhance the RAQ framework's ability to adapt codebook rates without compromising reconstruction fidelity.

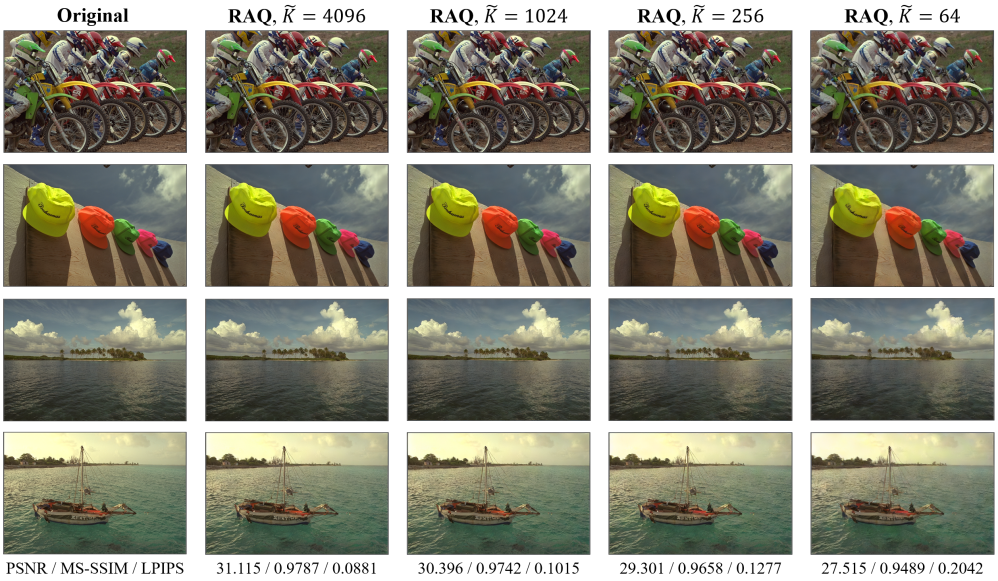

Figure 8: **Reconstructed images** for Kodak (Kodak, 1993) dataset at different rates.